Insights into the local interaction mechanisms between fermenting broken maize and various binder materials for anaerobic digester structures

Marie Giroudon, Cédric Perez, Matthieu Peyre Lavigne, Benjamin Erable, Christine Lors, Cédric Patapy, Alexandra Bertron

Insights into the local interaction mechanisms between fermenting broken maize and various binder materials for anaerobic digester structures

Marie Giroudon[1,2], Cédric Perez[3,4,5], Matthieu Peyre Lavigne[2], Benjamin Erable[3], Christine Lors[4,5], Cédric Patapy[1], Alexandra Bertron[1,*]

1. LMDC, Université de Toulouse, UPS, INSA Toulouse, France
2. TBI, Université de Toulouse, CNRS, INRA, INSA, Toulouse, France
3. Laboratoire de Génie Chimique, Université de Toulouse, CNRS, INPT, UPS, Toulouse, France
4. IMT Lille Douai, Institut Mines Télécom, Univ. Lille, Centre for Materials and Processes, F-59000 Lille, France
5. Univ. Lille, Institut Mines Télécom, Univ. Artois, Junia, ULR 4515 - LGCgE, Laboratoire de Génie Civil et géo-Environnement, F-5900 Lille, France

* Corresponding author: bertron@insa-toulouse.fr

Highlights

- Cement matrices face biodeterioration but have little effect on anaerobic digestion
- CH_4 production was similar in all BMP reactors (with/without binder materials)
- Alkali-activated metakaolin shows a thinner chemically modified layer
- Metakaolin paste impacts the digestion in terms of [NH_4^+], biomass nature, and pH
- The sessile and planktonic microbial communities are different

Abstract

Concrete structures of anaerobic digestion plants face chemically aggressive conditions due to the contact with the complex liquid fraction of the fermenting biowaste. This paper aims to determine the biogeochemical dynamic interaction phenomena at play between the biowaste and cementitious matrices at the local scale, and to identify durable binders in such environments. Binder materials

likely to show increased durability – slag and calcium aluminate cement, and a metakaolin-based alkali-activated geopolymer – and a reference Portland cement were inserted into sealed bioeactors during 5 cycles (245 days) of broken maize anaerobic digestion. Cementitious pastes suffered chemical and mineralogical alteration related mainly to carbonation and leaching. However, they had no negative impact on the bioprocess in terms of pH, metabolic evolution of volatile fatty acids and NH_4^+, planktonic microbial community composition or CH_4 production. In all reactors, the microbial community was able to perform the anaerobic digestion successfully. The MKAA was only slightly altered in its outermost layer. Its presence in the biowaste induced lower NH_4^+ concentrations, a slightly higher pH and a marked shift in the microbial community, but CH_4 total production was not affected. Substantial enrichment of acid forming bacteria, especially members of the genus *Clostridium*, was observed in the biofilm formed on all materials.

Keywords: Anaerobic digestion, cementitious materials, geopolymer, durability, biodeterioration, biofilm

Graphical abstract

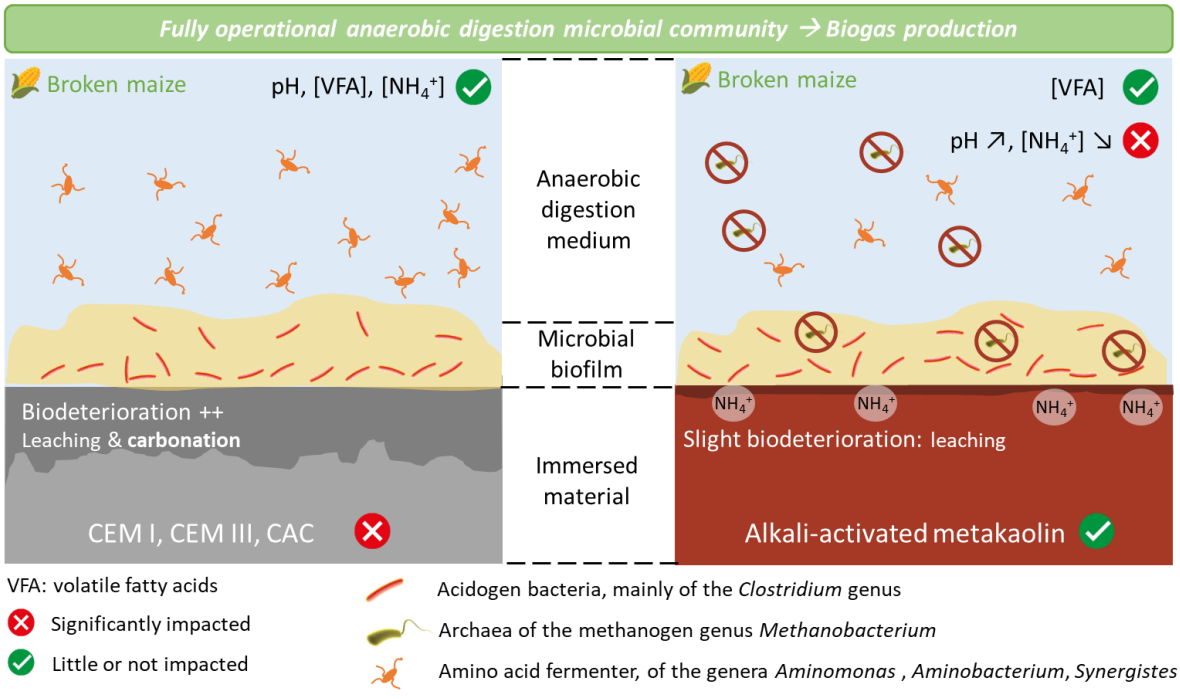

1 Introduction

Anaerobic digestion (AD) is the process of transforming organic matter into a methane (CH_4)-rich gas (the biogas) and a moist conditioner and fertilizer (the digestate) by anaerobic microorganisms. In the current context of sustainable transition towards low carbon renewable energies and reduction of greenhouse gas emissions into the atmosphere, the development of the sector is being encouraged in Europe and the number of industrial installations is growing. As an illustration, in France, the objective of the Pluriannual Energy Programme is to reach the target of including 7 % to 10 % of biogas in the total gas consumption by 2030 (Ministère de la transition écologique et solidaire, 2020).

On an industrial scale, the AD bioprocess is implemented in anaerobic digesters, i.e. fermentation plants, which are mainly made of concrete because this material is economical, easy to implement, waterproof, and has a good thermal inertia. While the upper part of the structure, in contact with the biogas, is often protected from the aggressiveness of the environment by liners (Nathalie Bachmann, 2013), in the lower part, the concrete is in direct contact with the biowaste undergoing digestion. Concrete structures that are thus directly exposed to the fermenting biowaste experience severe deterioration (Giroudon et al., 2021a; Koenig and Dehn, 2016; Perez et al., 2021; Voegel et al., 2019, 2016) which could affect the sustainability of the structures and their durability, with both economic and environmental consequences.

In more detail, the microbiologically driven AD bioprocess requires the succession of four steps of biowaste degradation under anaerobic conditions: hydrolysis, acidogenesis, acetogenesis and methanogenesis (Batstone et al., 2002; Evans and Furlong, 2003). During the first step, macromolecules of biowaste are broken into smaller molecules. These compounds of lower molecular weight are then fermented by acidogenic bacteria during the second step, leading to the specific production of volatile fatty acids (VFA) (mainly propionic, acetic and butyric acids). During the following step of acetogenesis, the products of the previous step are converted into acetate, H_2 and

CO_2 (Bond and Templeton, 2011). Finally, CO_2 and CH_4 are produced through two distinct pathways during methanogenesis: the hydrogenotrophic pathway produces CH_4 from H_2 and CO_2; and the acetoclastic pathway uses acetate as a precursor substrate (Krakat et al., 2010). All the AD reaction steps are carried out by microorganisms that can adopt clustered structures in the form of sludge, aggregates, or biofilms, which allow close interaction and cooperation between the microbial populations involved in the four reaction stages. Some of the microbial metabolites produced in the AD process, especially VFA, dissolved CO_2, and NH_4^+ ions (contained directly in some waste and/or produced along with VFA during acidogenesis (Meegoda et al., 2018)) are known to be aggressive for concrete (Giroudon et al., 2021a; Koenig and Dehn, 2016; Perez et al., 2021; Voegel et al., 2019) and are present in varying proportions. Moreover, the action of microorganisms organised in biofilms on the concrete surface can increase the local concentration of metabolites and locally accentuate the aggressiveness of the environment and thus the degradation of the concrete (Magniont et al., 2011).

With a view to enhancing the durability of concrete in this expanding industrial sector, this study aims at an extensive understanding of the biogeochemical interactions between cement matrices and the liquid fraction of biowaste in AD. On the one hand, the impact of the presence of different binder materials on the performance of the AD bioprocess is evaluated considering (i) the CH_4 production, (ii) the chemical composition of the liquid fraction in terms of VFA concentrations, NH_4^+ ion concentration and pH, and (iii) the microbial diversity of sessile and planktonic biomasses. On the other hand, the chemical and mineralogical changes of the binder materials previously exposed to the fermenting biowaste are also assessed. Cement pastes made of blast-furnace slag cement (CEM III), calcium aluminate cement (CAC), a metakaolin-based alkali-activated geopolymer (MKAA) likely to show increased durability in this medium (Bertron et al., 2007a; Drugă et al., 2018; Duan et al., 2015; Grengg et al., 2020; Gruyaert et al., 2012; Oueslati and Duchesne, 2012; Singh et al., 2015) and an ordinary Portland cement (CEM I) were immersed for 245 days in airtight biochemical methane potential (BMP) reactors (Holliger et al., 2016) inoculated with broken maize. This substrate was selected because it offers a high methanogenic potential (Bruni et al., 2010; Gerin et al., 2008) and

also because it allows the microbial production of a large amount of organic acids during the acidogenesis step, generating aggressive chemical conditions for the cement matrices. A high solid/liquid ratio (surface area of the material sample/liquid volume) was used in order to reproduce the local conditions occurring in the vicinity of the digester concrete walls.

2 Materials and methods

The experimental protocol was similar to the one developed and validated by Giroudon et al. (2021a) and is presented in Figure 1.

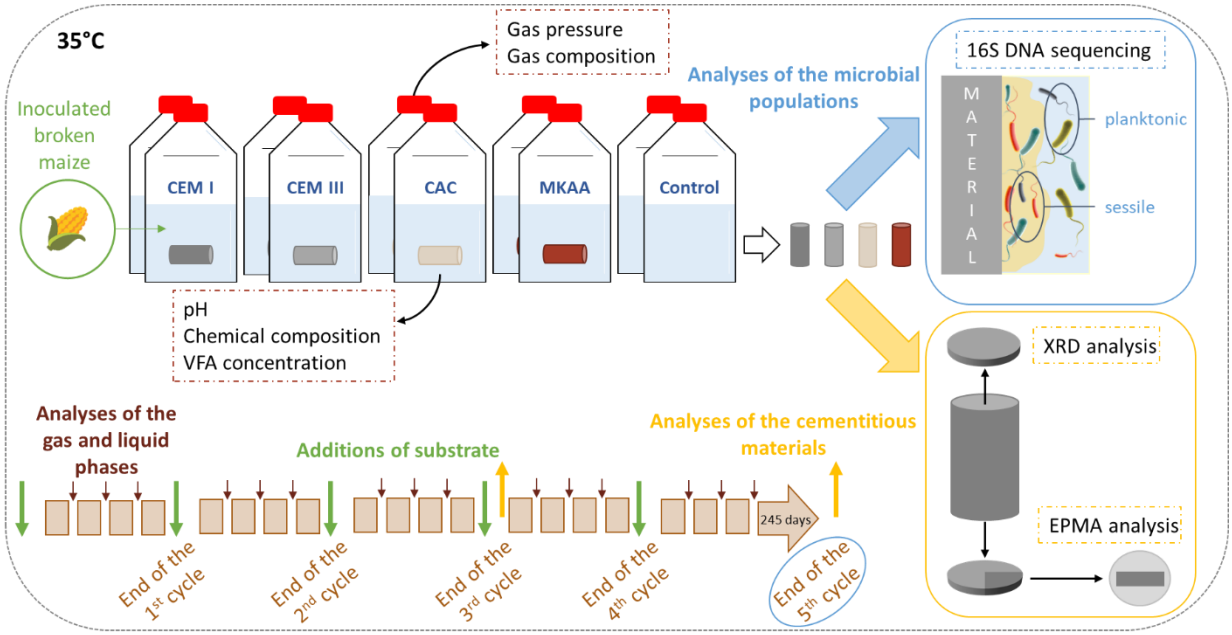

Figure 1: Schematic representation of the experimental protocol describing the samples, the experiments, and the temporal management of the solid, liquid and microbial fraction analyses, adapted from Giroudon et al. (2021a)

It consisted of immersing pastes made of ordinary Portland cement CEM I 52.5R (CEM I), CEM III/B 42.5N (CEM III), calcium aluminate cement, Calcoat ® RG (CAC), and a metakaolin-based alkali-activated (MKAA) paste, in reactors inoculated with broken maize at 35 °C, in order to reproduce anaerobic digestion during 5 cycles of digestion.

2.1 Binders

The cement pastes (CEM I, CEM III, CAC), called cementitious materials or cement pastes below, were poured with a water/binder ratio of 0.30. The MKAA geopolymer was made according to the procedure of Pouhet (2015) by using metakaolin, liquid sodium silicate (molar ratio $\frac{SiO_2}{Na_2O} = 1.7$) and water. Geopolymers are aluminosilicate materials formed by the activation of an aluminosilicate source, such as metakaolin, by a strongly basic alkaline solution (Pouhet et al., 2019).

The samples were made according to the procedure described in the study by Giroudon et al. (2021a), i.e., the paste specimens were mixed using the French standard NF EN 196-1 (2016) and cast in cylindrical moulds 75 mm high and 25 mm in diameter. They were cured in sealed plastic bags and were then exposed to the biowaste in AD.

The water porosities of the pastes were measured according to the NF P18-459 standard (AFNOR, 2010). The measurements show a significantly higher porosity of the MKAA paste (48.6 %) and a lower porosity of the CAC paste (24.0 %) in comparison with the CEM I and CEM III pastes, whose water porosity values were intermediate - about 32.0 % and 35.6 %, respectively.

2.2 Immersion of cement pastes in laboratory BMP reactors

The protocol of immersion consisted of immersing cement paste specimens in airtight BMP reactors (Holliger et al., 2016) containing 80 mL of microbial inoculum from an industrial biogas plant located in Haute-Garonne (France) and broken maize from a farm in Barcelonne-du-Gers (Gers, France) as the biowaste. For each kind of material, the experiment was carried out in duplicate with two BMP reactors each containing a sample. In addition, two control BMP reactors without material were also operated and monitored over the same period of time. The detailed protocol is presented in Giroudon et al. (2021a) (Section 2.1).

The mass of added broken maize increased with the cycles of AD (Table 1), in order to increase the aggressiveness of the medium with time. Each cycle of AD was considered complete when the gas

production in the BMP reactors stopped (Table 1). During the third cycle, once the biogas production was complete, the BMP reactors were kept at room temperature for 5.5 weeks because the laboratory closed for the summer break.

Table 1: Mass of broken maize added per cycle and duration of each cycle

	1st cycle	2nd cycle	3th cycle		4th cycle	5th cycle
Temperature	35°C	35°C	35°C	Room	35°C	35°C
Mass of broken maize added (g)	3	3	4		5	5
Duration of a cycle (weeks)	10	4.5	5	5.5	5	5

2.3 Analyses of liquid and gas fractions

Several times a week, the BMP reactors were shaken manually, the gas pressure was measured with a manometer, and gas and liquid were sampled using syringes. Gas samples were analysed using gas chromatography (GC Trace 1300 Thermofisher, Mobile phase Helium, Separation Column Hayssep N 60-80 1.0 m x 1/16, oven temperature 110°C, detector TCD) (O_2-N_2, H_2, CH_4, CO_2 and H_2S). pH was immediately measured in the liquid samples before they were centrifuged for 5 min (Eppendorf, Centrifuge 5430R, 4 °C, RCF 7197) and the supernatant was filtered through a 0.2 µm filter for further analysis. The NH_4^+ concentration was analysed by ion chromatography (Dionex Thermofisher ICS2000, Guard column AG19, IonPac CS12 3x250 mm, at 30 °C with eluent generator cartridge EGC III MSA for methanesulfonic acid) and the concentrations of some VFA (acetic, propionic, butyric, isobutyric, valeric, and isovaleric acids) were analysed by gas chromatography (Varian 3900/430, WAX column: length 15 m, external diameter 0.53 mm, thickness of the internal phase 1 µm, detector FID). In addition, gas and liquid compositions were used to calculate the aqueous inorganic CO_2 concentration in the liquid fraction using Henry's law considering a temperature of 35 °C and atmospheric pressure (values of the Henry's law constants from Batstone et al. (2002)).

2.4 Analyses of the changes in binder materials

The binder materials were removed from the BMP reactors after the 3rd and the 5th cycles and slices were sawn from their ends with a diamond saw. The remaining cylinders were re-immersed in the

BMP reactors as quickly as possible to continue the experiments, while the slices were used in analyses of the mineralogical and chemical changes following exposure to the fermenting biowaste. The mineralogical degradation in depth was assessed by qualitative X-Ray Diffraction (XRD) (Brucker Avance, Co cathode, 40 kV, 40 nA) by successively analysing and abrading the plane side of the slice until the core of the material was reached (initial mineralogical composition) (Bertron et al., 2005a). The chemical composition was quantitively characterized by Electron Probe Micro-Analysis (EPMA) (Cameca XFive, 15 kV, 20 nA) on polished sections: series of chemical punctual analyses (Ca, Si, Al, Fe, Mg, P and S) were performed from the surface in contact with the liquid fraction to the core of the specimen, avoiding the anhydrous grains. Calibrations were performed on synthetic natural controls before each run. The graphs are the combination of two chemical profiles in mass percentage of oxides from the same sample (each chemical profile consisting of a series of punctual chemical analyses, from the surface in contact with the biowaste to the sound core) and smoothed over 3 points for better readability, using a moving average (Bertron et al., 2009). Trend and smoothed curves were then established from these graphs.

2.5 Analysis of microbial populations

The protocol for collecting sessile microbial communities was adapted from Perez et al. (2021) in order to capture two distinct layers in the thickness of the biofilm successively**.** The "weakly adhered" biofilm was removed from the cementitious material surface by an immersion in phosphate buffered saline solution (PBS, 0.1 M, pH 7.4) for 15 minutes. The "strongly adhered" biofilm was removed by 3 minutes of sonication treatment (FB 15061 Fisher Scientific, ultrasonic frequency 37 Hz) in PBS. For both treatments, the entire PBS volume containing the detached biomass was then recovered. A 2 mL sample was also collected from the liquid fraction of each BMP reactor (Figure 1).

DNA was extracted from the three types of samples (“weakly adhered” biomass, “strongly adhered” biomass and planktonic biomass from the liquid fraction) with the Qiagen DNeasy power biofilm DNA extraction kit, according to the protocol described by the manufacturer. The extracted DNA was sent to RTL Genomics(Texas, USA), where the 16s rDNA was amplified using the 515F and 806R primers,

targeting both bacteria and archaea. Sequencing of the amplified DNA was also performed by RTL Genomics (USA) using a MiSeq Illumina platform (details of the amplification and sequencing protocols are available in the supplementary data). Data analysis for DNA quality, DNA sequence alignment, and clustering in operational taxonomic units and taxonomic assignment were also performed by RTL Genomics according to their protocol (available at https://rtlgenomics.com/amplicon-bioinformatics-pipeline). The sequencing raw sequence reads were published in the NCBI SRA database (accession: PRJNA758226; direct link: https://www.ncbi.nlm.nih.gov/Traces/study/?acc=PRJNA758226). The number of OTUs (Operational Taxonomic Units) identified at the taxonomic levels of species and genera were analysed statistically using the R software, (R Core Team, 2017). A heatmap was produced with the "Marray" package using Ward's classification method and the calculation of distance based on the correlation between the standardized abundance scores of each OTU. Principal component analyses (PCA) were performed with the "Factominer" and "Factoextra" packages.

3 Results

3.1 Characterization of the AD bioprocess with respect to the immersed binder

Table 2 gives the total production of CH_4 in each AD cycle for all BMP tests, with and without binder materials, and the cumulative total production at the end of the experiment.

Table 2: Total production of CH_4 ($NmL.g^{-1}$ of broken maize) at the end of each digestion cycle and cumulative total production at the end of the experiment (Total). Results are expressed as mean value of the two duplicates of BMP reactors ± the standard deviation.

	Control BMP reactors	CEM I	CEM III	CAC	MKAA	Mean values per cycle
	Production of CH_4 ($NmL.g^{-1}$ of broken maize)					
1st cycle	1530 ± 232	1439 ± 13	1579 ± 67	1379 ± 252	1336 ± 145	1453 ± 101
2nd cycle	1298 ± 88	1271 ± 91	1234 ± 48	1186 ± 136	1136 ± 131	1225 ± 65
3rd cycle	1308 ± 82	1214 ± 23	1270 ± 5	1283 ± 32	1178 ± 123	1251 ± 53
4th cycle	1005 ± 380	996 ± 290	1236 ± 81	1620 ± 556	1129 ± 39	1197 ± 256
5th cycle	1011 ± 174	1102 ± 45	1124 ± 3	1247 ± 46	1222 ± 35	1141 ± 96
Total	6152 ± 100	6022 ± 144	6392 ± 3	6715 ± 175	6001 ± 395	6267 ± 306

Despite the presence of the binder materials, the production of CH_4 was similar in all the BMP reactors during the whole experiment (Table 2). Even though the amount of broken maize biowaste was increased between the first and the last cycle, there was a slight decrease in the amount of CH_4 produced, probably due to the evolution, during storage, of the biowaste, the methanogenic potential of which decreased with time.

Figure 2 gives the evolution in time of the pH, the total concentration of VFA and the ammonium concentration in the liquid fraction of the BMP reactors.

The production of the different VFA in the different BMP reactors as a function of time is available in the supplementary materials (Appendix A). It shows that the production of acetic acid was predominant, and that the production and consumption of the different VFA was simultaneous in each type of BMP reactor.

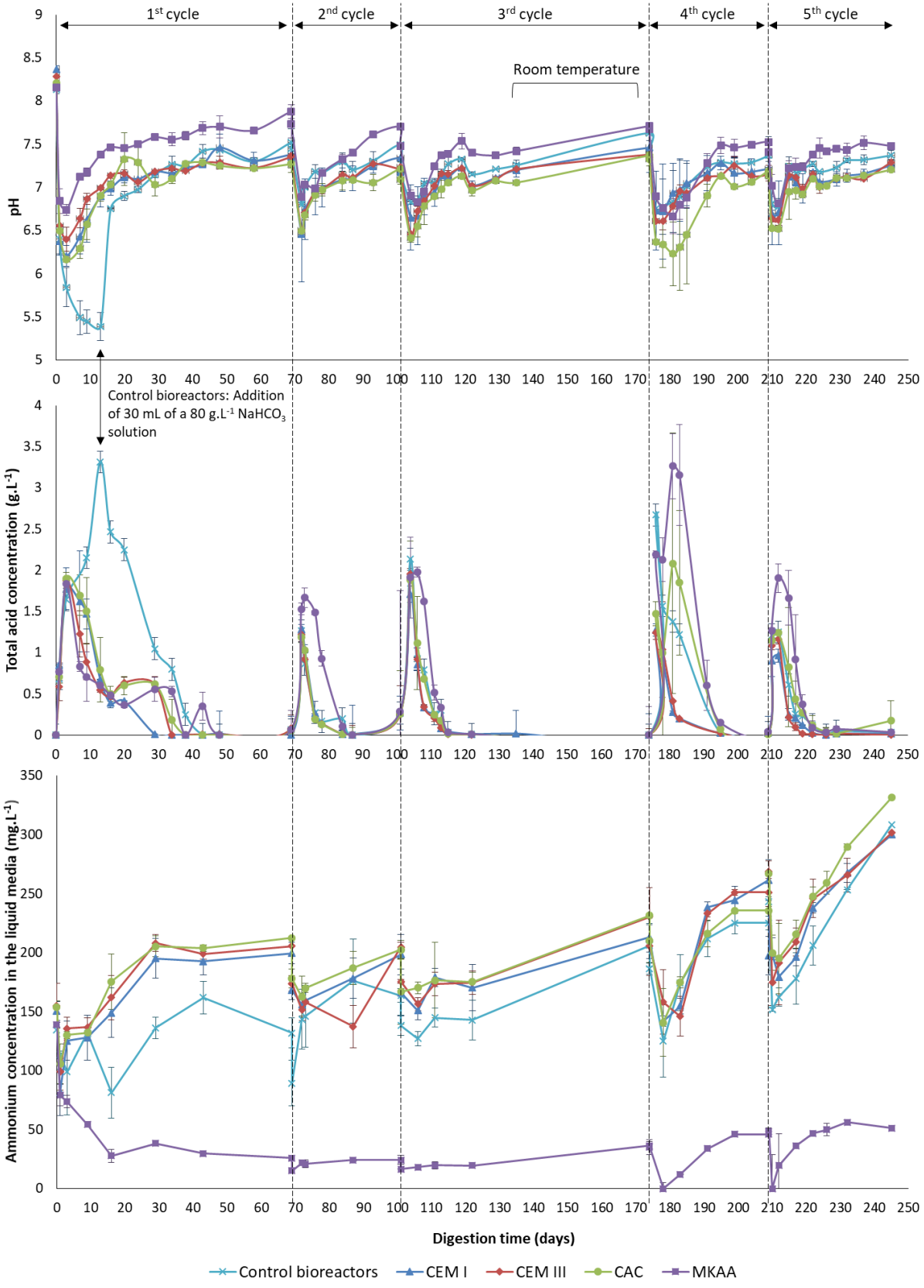

213

214 *Figure 2: Evolution of the pH, of the total VFA concentration and of the ammonium concentration during the five cycles of*
215 *AD in the BMP reactors, with or without binder materials. Mean values of the two duplicate BMP reactors are presented*
216 *with the standard deviations.*

At the beginning of the experiment (day 0), the pH values were very close in all the BMP reactors (8.2 ± 0.1). After three days, the pH had significantly decreased, reaching 5.8 ± 0.23, 6.2 ± 0.12, 6.4 ± 0.14, 6.2 ± 0.01, and 6.7 ± 0.06 in the control BMP reactors and the BMP reactors containing CEM I, CEM III, CAC and MKAA pastes, respectively. On the same day (day 3), the VFA concentration increased to 1.8 ± 0.1 $g.L^{-1}$. Thereafter, the VFA were consumed and the pH increased in the BMP reactors containing the binder materials. In the meantime, the pH continued to decrease in the control BMP reactors with no decrease of the acid concentration. Until day 13, the pH in these reactors continued to drop and reached 5.4 ± 0.20, with an extremely high total VFA concentration of 3.3 ± 0.23 $g.L^{-1}$. In order to avoid acidosis (acidic inhibition) in the BMP reactors, 30 mL of a $NaHCO_3$ solution (80 $g.L^{-1}$) was injected into each control reactor to increase the pH and promote favourable conditions for the AD bioprocess. The natural rise in pH in the BMP reactors containing the binder materials was due to the strong buffering effect of the cementitious and alkali-activated materials. The addition of the $NaHCO_3$ solution in the control reactors led to an increase of the pH and therefore allowed methanogenic microbial activity to take place (confirmed by the methane production rate measured, data not shown), leading to the consumption of the VFA and to the production of biogas.

Subsequently, the variations in pH were typical of a fed-batch AD bioprocess: the pH was between 7.0 and 7.5 in the steady state (suitable for AD microbial populations) and a decrease in pH occurred after each new addition of biowaste, due to the fast production of VFA. Starting from cycle 2, the microbial communities in the control BMP reactors adapted to the AD of broken maize, and the pH naturally rose after each addition of broken maize. The lower buffering effect of CAC material in comparison with the other materials induced a slightly lower pH during the experiment, which may have had an impact on the balance of microbial populations.

During the first cycle, among the BMP reactors containing binder materials, the pH was slightly higher in those containing the MKAA (about +0.5) while the VFA concentrations were similar. The pH

242 in these reactors remained that much higher during the whole experiment. However, with the
243 increase of the biowaste load from 3 to 5 g, the presence of MKAA induced a higher VFA
244 concentration and a slower consumption of acids. This could reflect a poorer efficiency of the
245 methanogenesis step. All VFA were, however, consumed at the end of each cycle and in all BMP
246 reactors.

247 The presence of the cementitious materials CEM I, CEM III and CAC did not significantly influence the
248 NH_4^+ concentration in the liquid fraction compared to that in the control BMP reactors. At the
249 beginning of each cycle, the evolution of the NH_4^+ concentration resulted from two opposite effects:
250 the addition of water led to a decrease in the NH_4^+ concentration by dilution, whereas the addition of
251 biowaste generated a gradual increase in NH_4^+ concentration. This increase was much more
252 significant during cycles 4 and 5, probably because the biowaste load was increased from 4 to 5 g.
253 The NH_4^+ concentrations in the BMP reactors containing the cementitious materials and the controls
254 were of the order of 150 to 300 $mg.L^{-1}$ during this experiment, which is much lower than the values
255 measured with bovine manure (approximately 750 $mg.L^{-1}$ at the end of the first cycle) (Giroudon et
256 al., 2021a). As highlighted in the study by Giroudon et al. (2021a), the presence of MKAA induced
257 significantly lower NH_4^+ concentrations (between 0 and 50 $mg.L^{-1}$), probably due to the NH_4^+
258 adsorption capacity of this material.

259 In the control BMP reactors, the sodium concentration increased sharply between the start of the
260 first cycle (64.7 ± 2.7 $mg.L^{-1}$) and the start of the second cycle (867.7 ± 22.0 $mg.L^{-1}$) due to the
261 addition of the $NaHCO_3$ solution on the 13th day (Table 3). Subsequently, the sodium concentration
262 decreased slightly during the experiment, from 867.7 ± 22.0 to 721.3 ± 13.2 $mg.L^{-1}$. This decrease was
263 the consequence of a dilution effect due to the addition of water at the beginning of each cycle, in
264 order to balance the volume losses related to liquid fraction sampling. Similar salinity values were
265 observed for the BMP reactors containing the CEM I, CEM III and CAC: the sodium concentrations
266 were between 74.0 ± 5.7 and 93.2 ± 2.1 $mg.L^{-1}$. The MKAA BMP reactors showed the highest salinity

values (about 1500 mg.L^{-1} of sodium in solution) because MKAA were activated with sodium silicate, and thus released a larger quantity of sodium.

Table 3: Concentrations of Na^+ and salinity ($[Na^+] + [K^+] + [PO_4^{3-}] + [Mg^{2+}] + [Ca^{2+}]$) in the liquid fraction of the BMP reactors at the start of each cycle (after the addition of water and maize), with or without the binder materials. Results are expressed as mean value of the two duplicates of BMP reactors ± the standard deviation.

		Start of the 1st cycle	Start of the 2nd cycle	Start of the 3rd cycle	Start of the 4th cycle	Start of the 5th cycle
$[Na^+]$ mg.L^{-1}	**Control**	64.7 ± 2.7	867.7 ± 22.0	818.4 ± 4.8	763.1 ± 3.3	721.3 ± 13.2
	CEM I	74.0 ± 5.7	90.2 ± 8.7	90.5 ± 0.6	93.2 ± 2.1	86.1 ± 5.7
	CEM III	77.4 ± 6.3	86.9 ± 4.0	85.9 ± 0.9	87.1 ± 4.6	79.5 ± 0.8
	CAC	73.2 ± 2.8	89.4 ± 3.6	93.2 ± 2.2	89.6 ± 3.7	78.6 ± 2.2
	MKAA	100.1 ± 4.4	1431.1 ± 26.7	1533.4 ± 1.8	1554.7 ± 26.3	1519.3 ± 3.1
Salinity mg.L^{-1}	**Control**	475.8 ± 13.4	1230.5 ± 314.9	1462.7 ± 91.5	1132.4 ± 31.2	1115.5 ± 34.5
	CEM I	537.1 ± 38.8	957.0 ± 35.5	1048.9 ± 32.4	848.1 ± 85.3	829.8 ± 147.7
	CEM III	572.1 ± 52.3	859.6 ± 37.5	936.7 ± 38.7	627.4 ± 14.6	523.0 ± 178.0
	CAC	520.4 ± 10.3	828.6 ± 30.3	904.8 ± 31.0	679.8 ± 33.4	699.6 ± 62.4
	MKAA	532.3 ± 32.3	1579.3 ± 57.8	1703.8 ± 14.8	1656.3 ± 31.4	1609.1 ± 7.8

3.2 Microbial composition of sessile and planktonic biomasses

The clustering by similarity shown on Figure 3 allows different groups and subgroups to be distinguished within the samples on the X axis and the OTUs grouped by genera on the Y axis. A grouping according to the type of material used in the BMP reactor was observed: the MKAA group is clustered on the right of the Figure 3 and all the other materials and the negative sample, without material, are mostly grouped on the left side of this figure. Subgroups formed in accordance with the origin of the microorganisms samplings. Groups of planktonic and sessile samples were clearly divided. Concerning the grouping of the identified OTUs, there were also groups and subgroups. However, no strong relation was observed between the groups of samples and the group of OTUs. This classification method does not highlight the relationships between the OTUs, the type of samples and the type of material used.

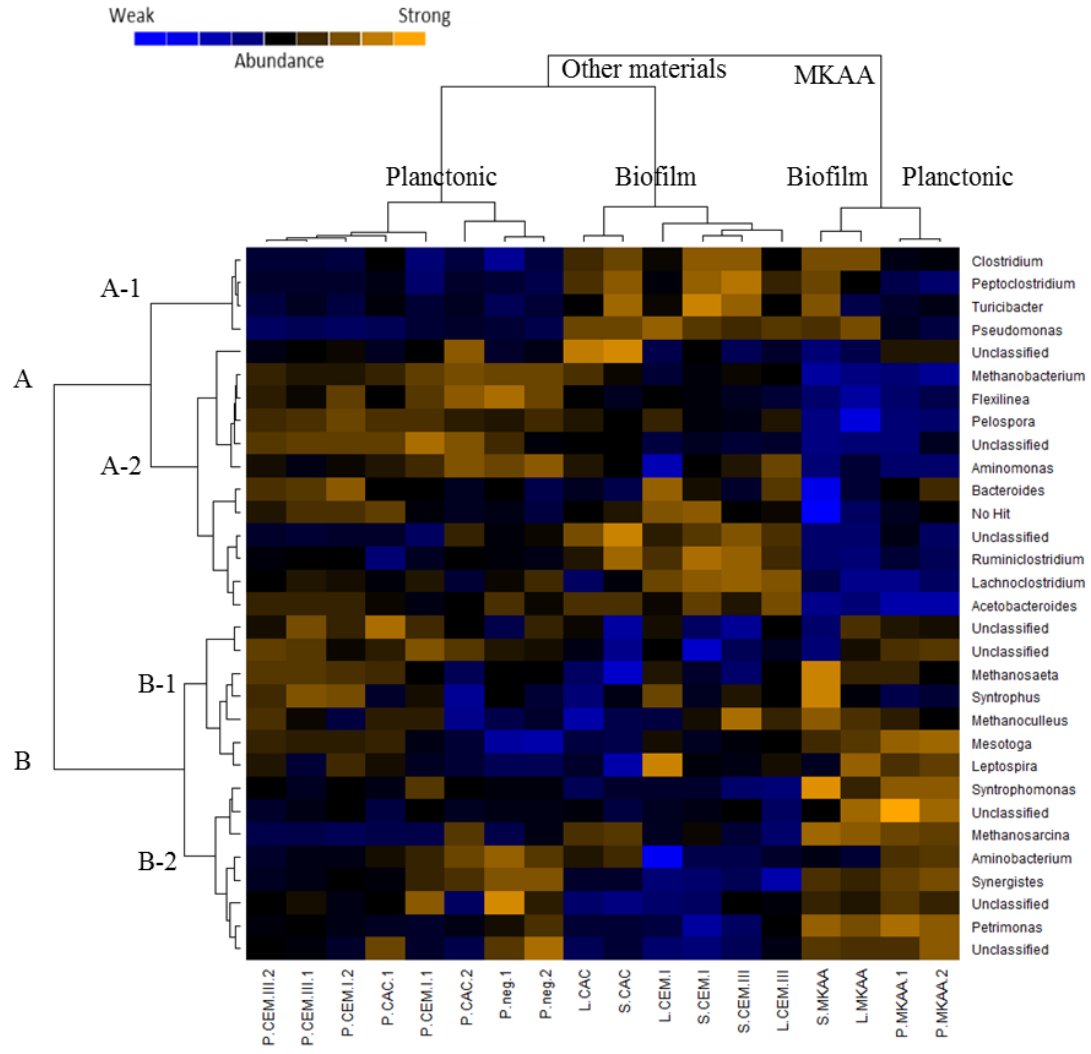

Figure 3: Heatmap with colour scale of the next generation sequencing of the 16S DNA from planktonic biomass samples and "poorly" and "strongly" adhered biomass taken from the surface of cementitious material samples, and after 5 cycles of anaerobic digestion – L: weakly adhered biofilm; S: Strongly adhered biofilm; P: Planktonic; only OTU genera with an abundance of at least 1% in at least one sample are shown

In order to assess these relationships, a principal component analysis (PCA) was carried out (Figure 4). Microbial samples are categorized according to the binder material used and the origin of the samples. The samples found on the left side of dimension 1 axis of Figure 4 all belong to the BMP reactors where MKAA (in blue) was immersed, while all the other samples are grouped on the right side of dimension 1 axis. The first PC, which explains 33.7 % of the global variability, is thus linked to the presence/absence of MKAA.

The second PC, explaining 25.6 % of the variability, is correlated with the origin of samples, since the strongly adhered biofilm samples (squares) are on the bottom part of dimension 2 axis, the liquid

297 samples (circles) on the top part, and the weakly adhered biofilm samples (triangles) are situated
298 between these two groups. So, the second PC is highly correlated with the origin of the microbial
299 samples and samples positionned towards the top of the dimension 2 axis should be the microbial
300 populations that were situated the closest to the cementitious material surfaces. Also, the
301 populations from the weakly adhered biomass should include a mix between the microbial
302 populations of the other two groups.

303 Therefore, the data presented can mainly be categorised according to two main criteria, which are
304 affiliated with the two CPs highlighted in Figure 4: firstly, the location of the sample, i.e. liquid or
305 weakly/strongly attached biomass and, secondly, the material exposed, i.e. MKAA binder or all other
306 binder materials tested.

307 It is interesting to look at Figure 3 while looking for the specific OTU genera found in these groups.
308 Several microbial genera appear more likely to be detected in the MKAA samples. These are the
309 acetogen genera *Petrimonas* and *Syntrophomonas* (T. E. Board, 2015; Sekiguchi, 2015). As for the
310 samples without MKAA: the genera *Methanobacterium* (methanogen), *Pelospora*, *Bacteroides*,
311 *Ruminoclostridium*, *Lachnoclostridium*, *Aminomona*s, *Flexilinea* (acidogens) and *Acetobacteroides*
312 (acetogen) are more abundant in those samples (Baena et al., 2015; Schink, 2015; Su et al., 2014;
313 Tourlousse and Sekiguchi, 2018; Venkiteshwaran et al., 2015).

314 When considering the other main criteria categorising our data, some kinds of OTUs were found
315 more predominantly in the biofilm samples. These genera, identified as *Clostridium,*
316 *Peptoclostridium, Pseudomonas* and *Turicibacter* (acidogen) (Bosshard, 2015), are the members of
317 the A-1 group (Figure 3). The *Pseudomonas* genus mainly contains CO_2-producing respiring bacteria,
318 known for their ability to form biofilms (Yoon et al., 2002). Also, among these four cited genera, the
319 acidogen genera *Clostridium*, *Peptoclostridium* and *Turicibacter* were more abundant in the strongly
320 adhered biofilm than in the loosely adhered one. As for the genera associated with the planktonic

lifestyle, the *Aminobacterium* genus and the *Synergistes* genus are both amino acid fermenters (E. Board, 2015).

The same clustering by similarities, initially presented at the genus level in Figure 3, was also performed at the level of the microbial species. The results are available as supplementary data (Appendix B). This clustering based on comparison at the microbial species level resulted in findings almost identical to those already shown in Figure 3. The genus *Clostridium* was highly represented, 14 OTUs being identified as belonging to this specific bacterial genus. The presence of each of these OTUs was significantly higher in the biofilm samples regardless of the type of binder material. This confirms the predisposition of this genus to widely form biofilms on surface materials. Among the methanogenenic population, 4 genera were identified: *Methanobacterium*, *Methanosarcina*, *Methanoculleus* and *Methanosaeta*. *Methanosarcina*, *Methanoculleus* and *Methanosaeta* were present in all the microbial samples in both the planktonic and biofilm samples. However, the hydrogenotrophic methanogens, represented by the *Methanobacterium* genus, were almost absent in the MKAA samples. The amino acid fermenter genera, *Synergistes*, *Aminobacterium* and *Aminomonas,* leading to the release of NH_4^+ ions, were more often detected in the liquid fraction than in the biofilm.

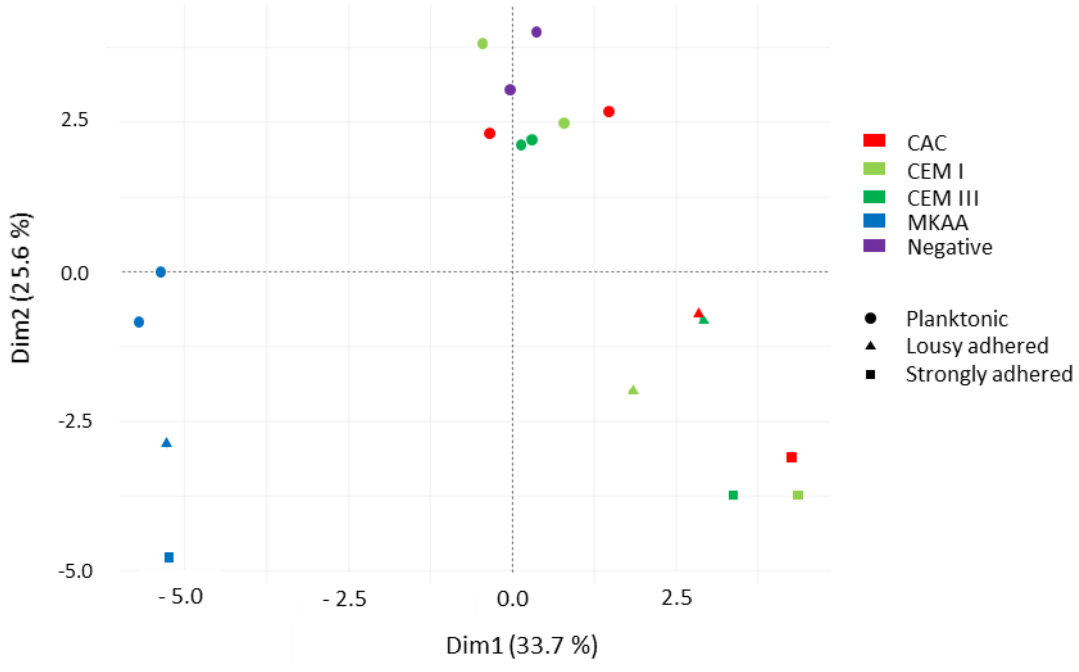

Figure 4: PCA of microbial communities found in anaerobic digestion biomass samples and representation according to either the type of material or the location of the biomass sample – Distribution of all the samples according to the two main Principal Components (PC)

3.3 Chemical and mineralogical changes in the binder materials

The mineralogical and chemical changes of CAC pastes after 3 and 5 cycles of immersion in the fermenting broken maize are available in the Supplementary materials (Appendix C) since the effect of biodeterioration only marginally modified this material throughout the experiment. The mechanisms explaining these moderate mineralogical and chemical evolutions under AD conditions have already been described in detail in the work of Voegel et al.(2019).

For better readability, the results for the CEM I, CEM III and MKAA are presented in the form of trend graphs. Original data (CEM I and CEM III after 5 cycles of AD) are provided as Supplementary materials (Appendix D, Appendix E, Appendix F and Appendix G).

3.3.1 CEM I

Figure 5 shows the chemical and mineralogical features of CEM I pastes resulting from 3 and 5 cycles of immersion in the fermenting broken maize. The measurements were carried out respectively by EPMA and XRD, as a function of the distance to the surface of the CEM I paste in contact with the fermenting biowaste. The EPMA analysis highlighted three main zones after 3 cycles and 4 main zones after the 5^{th} cycle. The sound paste was mainly made of calcium (50 %) and silicon (17 %) with minor amounts of aluminium, sulfur and iron. The mineralogical analyses showed the presence of typical hydrated (portlandite, ettringite) and anhydrous (C_2S, C_3S, brownmillerite, C_3A) crystallized phases of a Portland cement-based hydrated matrix. The material mainly underwent decalcification with a progressive decrease in the CaO content together with some dissolution (decrease of the

362 silicon and aluminium contents and dissolution of the Ca-bearing phases, mainly CH[1]) associated with
363 the carbonation of the outer layer of the CEM I paste (zones 3 and 2) with the precipitation of calcite
364 and vaterite. Additionally, an enrichment in exogenous phosphorus, probably supplied by the
365 fermenting biowaste, was spotted in the external zone. After 3 and 5 cycles, the sound zone was
366 identified at about 600 µm deep. The main difference between these two limits was the presence of
367 an intermediate zone spotted after 5 cycles (zone 3), between 100 and 300 µm deep, where calcium
368 and silicon contents remained stable while the sulfur content fell to 0 %.

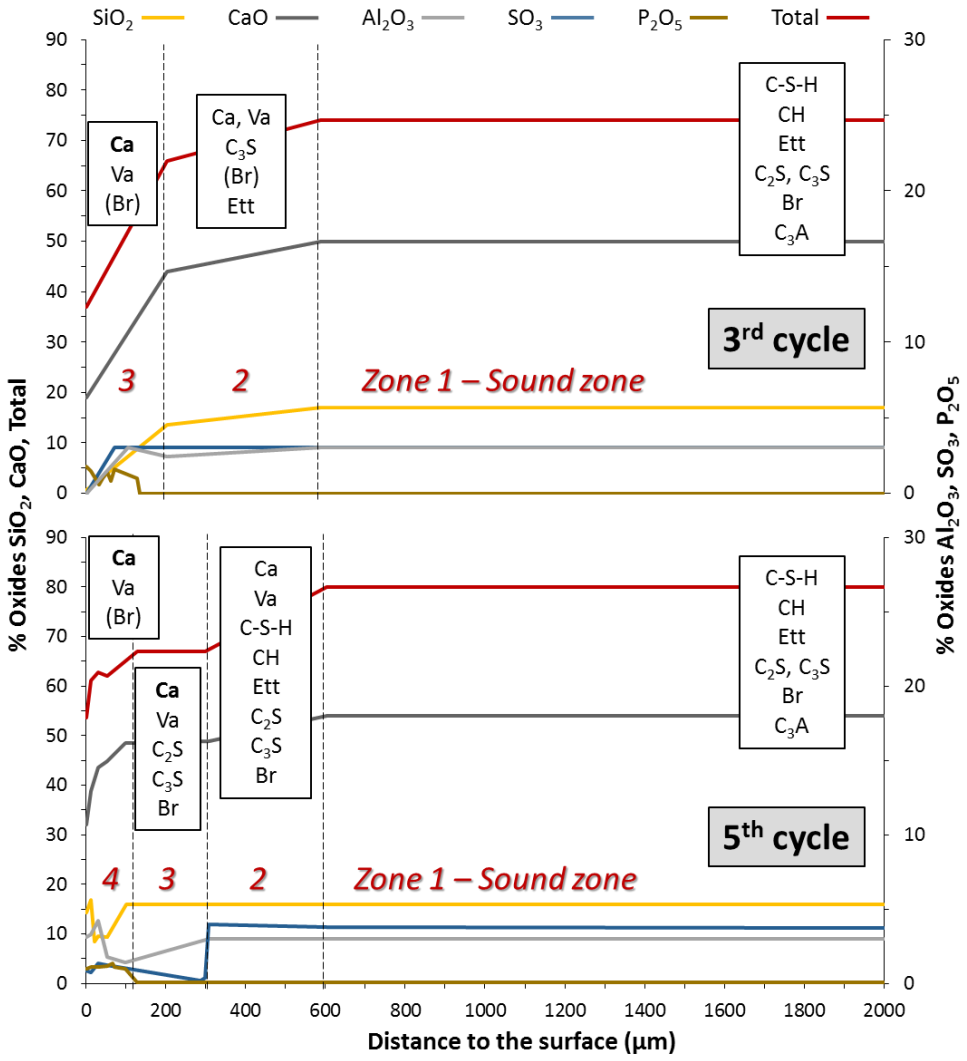

369

370 *Figure 5: Schematic representation of chemical composition of oxides and mineralogical composition (analysed by EPMA*
371 *and XRD, respectively) of the CEM I pastes after 3 and 5 cycles of exposure to fermenting broken maize – Ett: ettringite; Ca:*

[1] Cement chemistry shorthand notations: A = Al_2O_3, C = CaO, F = Fe_2O_3, H = H_2O, M = MgO, S = SiO_2

calcite; Va: vaterite; Br: brownmillerite – Bold characters = intensification of the XRD signal in comparison with the deeper zone; Parentheses = significantly lower intensity of the XRD signal in comparison with the main phase

3.3.2 CEM III

The sound CEM III paste was mainly made of calcium, silicon and aluminium with lower amounts of sulfur and magnesium (Figure 6). The mineralogical analyses showed the same main crystalline phases as for the CEM I paste. After 3 cycles, an enrichment in calcium was observed between 400 µm and 1200 µm, together with a slight enrichment in sulfur, even though no mineralogical changes were observed. The decalcification of the paste stopped at about 400 µm deep, and the sulfur content dropped to a value close to 0 % (zone 3). The decrease of all the oxide contents (zone 4) and the phosphorus enrichment (zone 5) were observed in the external zones. The mineralogical analyses showed the carbonation of the CEM III paste with the presence of calcium carbonates calcite and vaterite.

After 5 cycles, an enrichment in sulfur was observed between 600 and 1200 µm deep, together with the decalcification of the cement matrix (zone 4). Between 270 and 600 µm (zone 3), the calcium content increased, probably due to the carbonation of the paste, whereas the total oxide content, as well as the aluminium and the silicon contents, decreased. Once again, an intermediate zone (zone 2) was marked by the stagnation of the calcium, aluminium and silicon contents whereas the sulfur content dropped to 0 %, this time with an enrichment in phosphorus. The external zone showed drops in the major oxide contents whereas a new enrichment in phosphorus was seen (zone 1). The main crystalline phases were calcite and vaterite. For both limits, the modified depths of the CEM III paste were significantly higher than for the CEM I paste (1200 µm vs. 600 µm respectively).

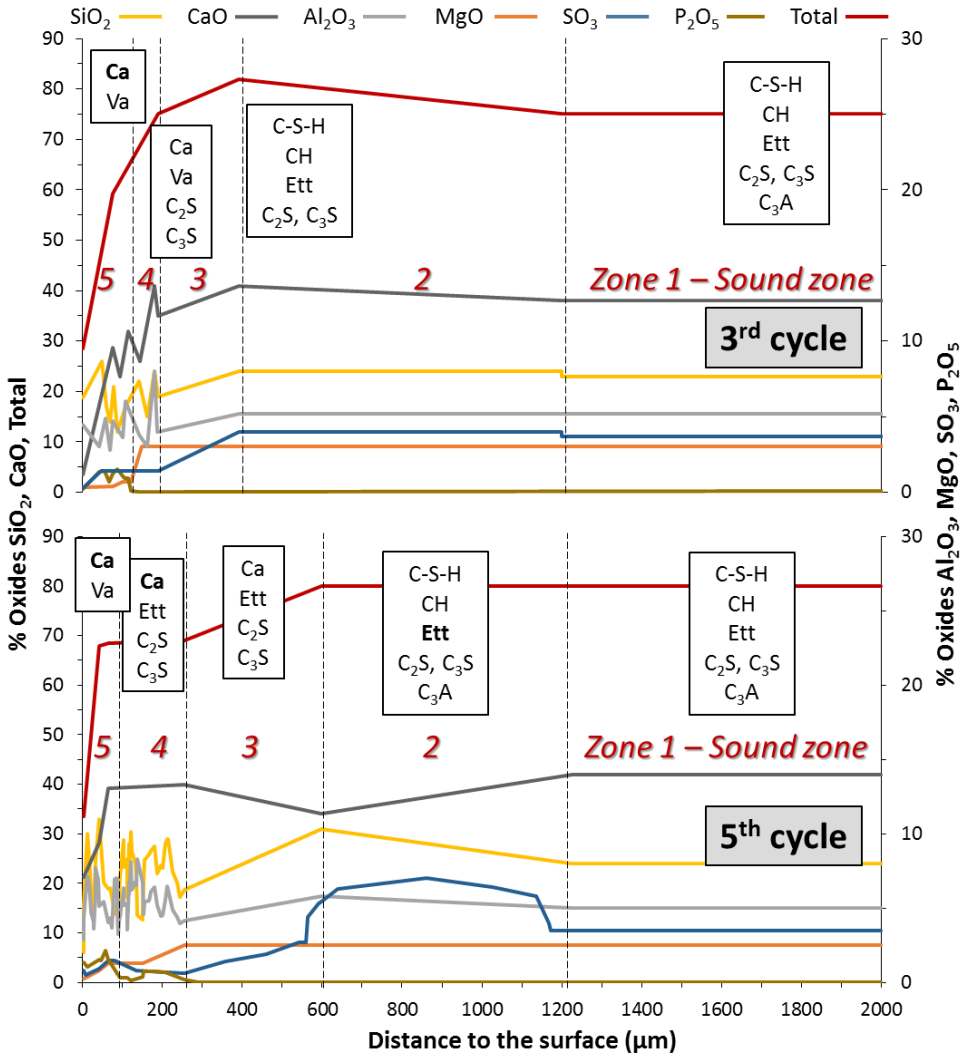

Figure 6: Schematic representation of chemical composition of oxides and mineralogical composition (analysed by EPMA and XRD, respectively) of the CEM III pastes after 3 and 5 cycles of exposure to fermenting broken maize– Ett: ettringite; Ca: calcite; Va: vaterite; Br: brownmillerite – Bold characters = intensification of the XRD signal in comparison with the deeper zone

3.3.3 MKAA

Figure 7 shows the chemical composition profiles of the MKAA paste together with the mineralogical phases identified. Because of the amorphous nature of the metakaolin and associated products of reaction, the XRD analyses did not show any mineralogical changes between the sound zone and the external part exposed to the aggressive environment. Only a thin outer fringe (100 and 180 µm wide respectively after the 3rd and 5th cycles) was significantly chemically modified, probably due to the dissolution of the paste. A drop in the potassium content was observed only in the degraded outer zone, around the outer 100 µm. Zone 1 bis showed the increase in the phosphorus content. After the

third cycle, this also corresponded to the increase in the sodium content just before its decrease in the outer zone, corresponding to its release into the liquid fraction. For the MKAA, it seems that the sodium contents in the solid varied greatly according to the depth, and the trends also varied depending on the samples. However, the decrease in the sodium content, like that of potassium, occurred only in the last micrometres (about 100 µm).

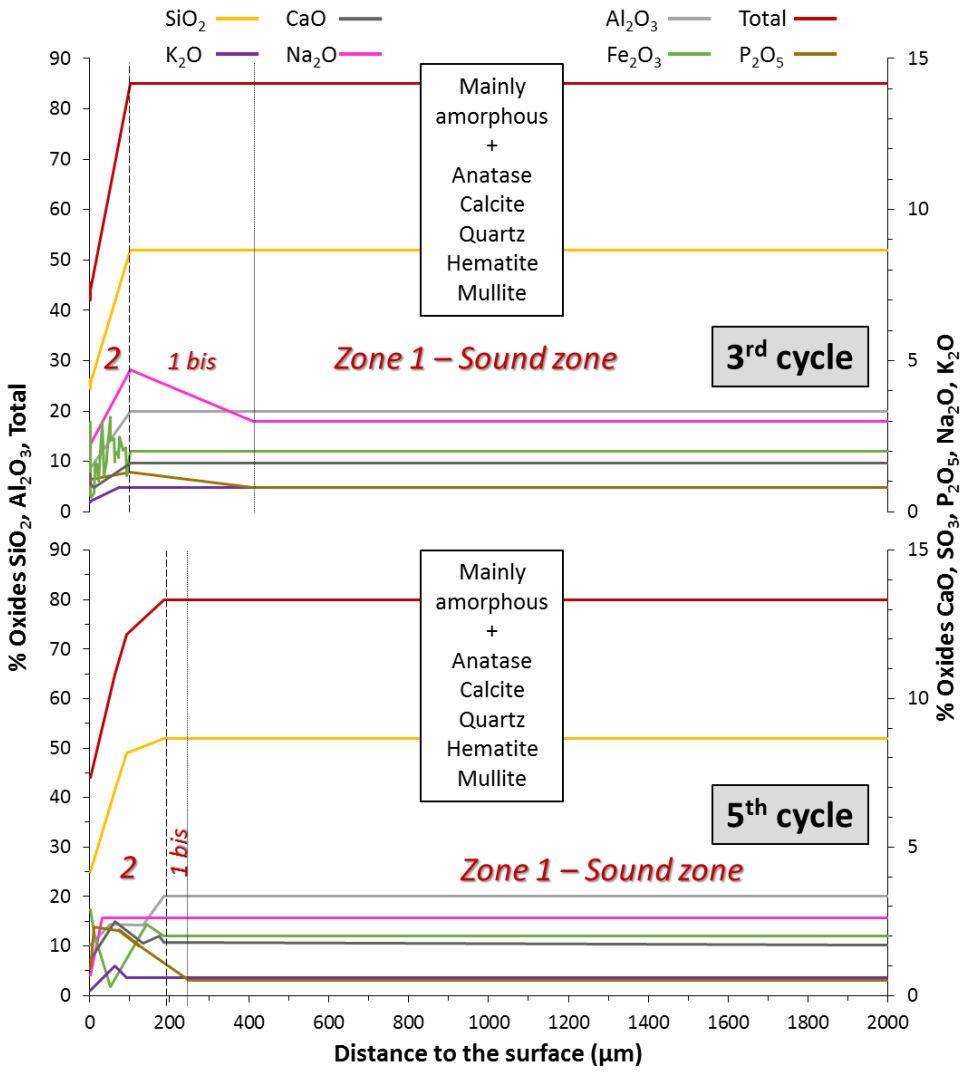

Figure 7: Schematic representation of chemical composition of oxides and mineralogical composition (analysed by EPMA and XRD, respectively) of the MKAA pastes after 3 and 5 cycles of exposure to fermenting broken maize

3.3.4 Relative performances of the binders

During the experiment (5 AD cycles, 245 days of exposition), the CEM I and CEM III pastes showed greater chemical and mineralogical changes than the MKAA pastes, in particular linked to the decalcification of the cement matrix and the dissolution of the initial mineralogical phases. In addition, the modified depths of the CEM III paste were much greater than in other materials at the end of the experiment. The MKAA samples appeared to show very stable behaviour against biochemical attack, with a very shallow modified depth. Thus, a trend of chemical stability of mineralogical phases to attack by digesting biowaste can be established on the basis of the results of this study: CEM III < CEM I < MKAA.

4 Discussion

4.1 Effect of the AD bioprocess on the binder materials

Cementitious materials are porous and strongly basic reactive media that experience a chemical attack by the liquid fraction of the biowaste in AD, thus releasing chemical compounds that could disrupt microbial activities. In this study, despite the high solid/liquid ratio used, it was observed that the presence of the binder materials did not decrease the efficiency of the AD, the CH_4 production being similar in all BMP reactors.

These observations are different from what had been observed by Giroudon et al. (2021a) who, in a slightly different way, studied the impact of cementitious materials on the AD of cattle manure. However, they are consistent with the studies of Voegel et al. (2016, 2019b), where the authors focused on the AD of collective food catering waste in laboratory conditions. With or without the presence of cementitious materials, they described similar values and trends for the pH and for the production kinetics of VFA, even though the CH_4 production was not measured. Broken maize has a much greater methanogenic potential than cattle manure (French Chamber of Agriculture, 2010) and, above all, faster hydrolysis. Thus, much higher VFA concentrations were observed at the start of

440 the cycles (maximum of 0.35 $g.L^{-1}$ for cattle manure and 1.8 $g.L^{-1}$ for broken maize in the first cycle),
441 linked to a strong acidification of the environment, as in the studies by Voegel et al. (2016, 2019b).
442 The transformation of this large amount of fermentable biowaste led to a production of CH_4
443 approximately 7.5 times greater than that obtained with cattle manure (data not shown).

444 For both biowastes (cattle manure and broken maize), the presence of the binder materials impacted
445 the AD bioprocess. In the case of AD of cattle manure, the alkalis of the materials (Na^+, K^+), released
446 during the first cycle, raised the pH and inhibited some of microorganisms implicated in the AD
447 bioprocess (acidogenic, acetogenic, and methanogenic populations). In the case of AD of broken
448 maize, the leaching of these alkalis counterbalanced the strong acidity of the liquid fraction, thus
449 avoiding the phenomenon of acidosis that appeared in the control BMP reactors during the first
450 cycle, and enabling the AD sequence to progress well.

451 In AD, NH_4^+ is classically produced by the degradation of proteins or urea (Kayhanian 1999; Yenigün
452 and Demirel 2013), which justifies the high concentrations of NH_4^+ during the AD of cattle manure
453 (approximately 750 $mg.L^{-1}$) (Giroudon et al., 2021a), while the concentrations did not exceed 350
454 $mg.L^{-1}$ with the broken maize. According to the pKa of the acid and conjugate base NH_4^+/NH_3, i.e.
455 9.25, the ammonia was mainly in the form of NH_4^+ ions in this experiment, with no possible stripping
456 in the gas phase. These low concentrations of NH_4^+ are below the concentrations known to
457 inhibit/impact the microbial digestion activity, since the lowest inhibition values collected from the
458 literature are of the order of 600 $mg.L^{-1}$ (Karthikeyan and Visvanathan, 2013).

459 In both experiments (broken maize vs. cattle manure), in pH conditions suitable for AD, the presence
460 of MKAA led to a significant decrease in the concentration of NH_4^+ ions. The hypotheses and possible
461 mechanisms between NH_4^+ ions and the MKAA are detailed in Giroudon et al. (2021b).

4.2 Microbial communities associated with binder materials

4.2.1 Microbial communities with sessile and planktonic lifestyles

In our study, a strong presence of the *Clostridium* genus was found in the biofilm and even more in the strongly adhered fraction of the biofilm, i.e. the layers closest to the solid material surface. A similar finding has already been documented for a microbial biofilm formed on cellulose particles during the anaerobic digestion of the particles in a batch process of particulate cellulose AD. Hydrolytic bacteria colonized the particles during the first 14 days, then their number decreased to be ultimately supplanted by methanogenic archaea (Song et al., 2005). In our study, the methanogenic OTUs were present in both sessile and planktonic communities. Our samples were exposed for almost 2.5 times as long as those of Perez et al. (2021), who recently compared the microbial diversity of microbial communities collected from a fermenting biowaste, inoculated early with activated sludge, and on CEM I cement pastes immersed in the same fermenting biowaste for up to 15 weeks at 37 °C. They found that acidogenic bacterial populations were enriched in the community colonizing the CEM I surface, especially members of the *Clostridium* genus. In the liquid fraction, methanogens and acetogens were predominant. The longer exposure time of binder materials in our study probably offered both planktonic and sessile communities the possibility to mix and form a thicker, hierarchically organized biofilm on binder surfaces, explaining why, in our case, methanogenic and acetogenic populations were present in the biofilm.

The presence of the genus *Clostridium* in the strongly adherent layers of the biofilm might be interpreted as being due to its rapid implantation occurring very early in the cycle of biofilm formation on the surface of the binders. Following its installation on the surface of the solid pastes, its acidogenic metabolism would then lower the pH on the binder surface and make the pH conditions more suitable for the integration of both methanogenic and acetogenic microorganisms in the biofilm community. Consequently, this scenario is particularly detrimental to the cementitious

material, as the high local production of microbial acids on the surface would promote the acid attack of the binder matrices and significantly increase the biodeterioration kinetics.

4.2.2 Material influence on the microbial communities

For all samples, regardless of the type of material, the microbial community identified corresponded to a community capable of performing the four steps of anaerobic digestion and is commonly found in anaerobic digestion environments (Venkiteshwaran et al., 2015).

A previous work immersing CAC, CEM I and CEM III cement pastes in a lab scale AD bioprocess system showed a short-term inhibition of the microbial colonization of CAC material that disappeared after 10 weeks (Voegel et al., 2020). In the present study, no significant difference between CAC samples and CEM I, CEM III and planktonic samples was observed. This tends to confirm that there is no inhibition caused by the CAC, for exposure times longer than 10 weeks (Voegel et al., 2020).

The specific change in the microbial community in relation to the presence of the MKAA material is most probably related to the lower NH_4^+ concentration observed in the reactors containing MKAA material. This drop in NH_4^+ concentration is the only environmental variable that differs when the AD batches with MKAA or with the other binder materials are compared. Sodium concentration was also different when the AD bioprocess evolution with MKAA and with the other materials were compared. But the values were really close to the concentration measured in the control. Although NH_4^+ is a very common inhibitor of the AD bioprocess at concentrations above 600 $mg.L^{-1}$ (Karthikeyan and Visvanathan, 2013), the effects of low NH_4^+ concentrations on AD microbial communities are not documented in the literature. It is therefore not entirely possible at this stage to state with absolute conviction that NH_4^+ is responsible for this marked shift in the microbial community. A dedicated comparative study involving dynamic monitoring of an anaerobic digestion microbial community exposed to low or high concentrations of NH_4^+ could help to confirm the key role of NH_4^+. Nevertheless, CH_4 production was approximately the same in all BMP reactors,

indicating that, although the material had an influence on the microbial populations, it did not affect the main function of anaerobic digestion.

4.3 Deterioration mechanisms of the material samples

4.3.1 CEM I and CEM III

Both CEM I and CEM III pastes showed mechanisms corresponding to a combination of leaching and carbonation, with a phosphorus enrichment in the external zone, as identified in other studies evaluating deterioration mechanisms of cementitious materials by biowaste in anaerobic digestion (Bertron et al., 2017; Giroudon et al., 2021a; Voegel et al., 2019, 2016). However, unlike the pastes immersed in inoculated cattle manure (Giroudon et al., 2021a), the CEM I and CEM III samples did not show identical degradation mechanisms, since particular chemical changes were observed on the CEM III pastes. Contrary to the findings of Koenig and Dehn's study (2016), where the use of low-clinker binders with blast-furnace slag in the liquid fraction of a pilot scale fermenter led to a reduction in depths of modification, the modified depths of the CEM III paste were twice those of CEM I.

The CEM I paste showed deterioration mechanisms similar to the ones encountered for acids with soluble salts and for NH_4^+ attacks, with a decalcification and gradual dissolution of the initial mineralogical phases (Bertron et al., 2004; Bertron and Duchesne, 2013; Duchesne and Bertron, 2013; Escadeillas, 2013). However, despite the high concentrations of VFA (maximum VFA concentrations between 1 and 3 $g.L^{-1}$ at the beginning of the cycles), it appears that carbonation played an important role in the chemical and mineralogical changes of the paste. Calcium carbonates were detected in the outer layers, and the degraded depth did not increase as the experiment progressed. This could be explained by the clogging of the cementitious matrix by calcium carbonates (Baroghel-Bouny et al., 2008; Shah et al., 2018), leading to a slowing of the ingress of aggressive agents'.

Carbonation phenomena are linked to the microbial production of CO_2 in the liquid fraction of the fermenting biowaste. Dissolved CO_2 reacts with calcium released by the dissolution of cementitious matrix phases to form calcium carbonates. However, the analyses of the liquid fraction of the fermenting broken maize showed concentrations of total inorganic carbon similar to or even lower than those reported by Giroudon et al.(2021a), with values of about 1000 $mg.L^{-1}$. At the equilibrium, for the experiment with broken maize, the total inorganic carbon concentrations in the liquid fraction were lower due to a lower concentration of CO_2 in the gas phase and a lower pH in the liquid fraction. However, the quantity of CH_4 produced in the course of the experiment was significantly higher in the case of the broken maize. Thus, even for lower observed concentrations of CO_2, its microbial production was actually much higher during the digestion of the broken maize, which induced a much greater flow of CO_2 in the liquid fraction in contact with the materials. This, in turn, could explain the predominant effect of carbonation in this environment. This was confirmed by experiments performed with chemical metabolites alone (Giroudon et al., 2021b) where the authors immersed Ordinary Portland Cement pastes in single-compound-based solutions.

Carbonation phenomena were also identified in the CEM III paste, but the modified depth increased significantly with time. The differences of behaviour between the CEM I and the CEM III pastes could be linked to the initial greater porosity of the CEM III paste or to the poorer performance of slag cements toward carbonation (Osborne, 1999).

In Portland based cements, portlandite is an abundant constituent of the paste and is the hydration product that reacts the most readily with carbon dioxide (Galan et al., 2015; Thiery et al., 2007). Its carbonation results in the precipitation of calcium carbonates in the pore network, decreasing the total pore volume and shifting the pore size distribution curve toward smaller pore diameters (Šavija and Luković, 2016). Moreover, the carbonation in Portland cement also causes a loss of pore connectivity (Han et al., 2015).

559 The C-S-H decomposition by carbonation consists of the decalcification of the C-S-H gel with the
560 decrease of the Ca/Si ratio and can lead to a silicate polymerisation and to the formation of an
561 amorphous silica gel and calcium carbonates (Li et al., 2017; Sanjuán et al., 2018; Šavija and Luković,
562 2016; Steiner et al., 2020). Furthermore, it appears that the C-S-H decomposition increases with
563 decreasing Ca/Si ratio (Sevelsted and Skibsted, 2015). For extensive decalcification, the precipitation
564 of calcium carbonate polymorphs and the formation of a silica gel result in significant shrinkage, loss
565 of cohesion, increase in the number of pores and increased porosity (Li et al., 2017; Nedeljković et
566 al., 2018; Puertas et al., 2006; Sanjuán et al., 2018).

567 The use of GGBS as a supplementary material leads to a reduced portlandite content and a lower
568 Ca/Si ratio in the C-S-H gel (Lothenbach et al., 2011). Thus, the carbonation of slag cements leads to a
569 decrease of their micro-mechanical properties (Nedeljković et al., 2018) and to the coarsening of
570 their pore structure (Ngala and Page, 1997; Šavija and Luković, 2016). Several authors have reported
571 extensive cracking and increases of the chloride diffusion coefficient and the oxygen permeability
572 with carbonation on blended cements (Borges et al., 2010; Ngala and Page, 1997).

573 Under these CO_2-rich conditions, CEM III cement based matrices, well-known for their interesting
574 performances against acid attacks (Bertron et al., 2005b; Gruyaert et al., 2012; Oueslati and
575 Duchesne, 2014) or in mainly acidic environments (Koenig and Dehn, 2016), seem more sensitive to
576 the aggressiveness of this environment than CEM I cement pastes do, as portlandite is present in
577 lower quantities in the CEM III pastes and does not play its role of a sacrificial phase generating
578 calcium carbonates via its reaction with CO_2. The C(-A)-S-H are thus attacked, which damages the
579 paste. The carbonation may have increased the porosity of the CEM III pastes and induced a greater
580 penetration of aggressive agents into the sample, which could explain the chemical and mineralogical
581 changes highlighted above and also the deeper penetration of phosphorous from the liquid fraction
582 into the material. Significant carbonation followed by acidification cycles could also have weakened
583 the material.

4.3.2 MKAA

MKAA pastes showed only a very low degraded zone over the last hundreds of microns, as in the previous study by Giroudon et al. (2021a) with cattle manure, and despite more aggressive conditions in terms of acid concentrations and CO_2 flow. The chemical profiles highlighted the dissolution of the matrix (Si, Al, Fe, Na), which has already been identified during acid attacks in other studies (Bakharev, 2005; Burciaga-Díaz and Escalante-García, 2012; Ukrainczyk and Vogt, 2020). Thus, in the case of MKAA, the acid attack seems to have a predominant effect. According to Burciaga-Díaz and Escalante-García (2012), the deterioration of the paste in an acidic environment is due to the destruction of the geopolymeric structure and the release of Na, Al and Si into the solution. Several authors (Bakharev, 2005; Burciaga-Díaz and Escalante-García, 2012) agree that it causes the breakdown of the aluminosilicate network of geopolymers. Nevertheless, in this environment, the MKAA did not show any sign of intense cracks or lack of mechanical strength and showed really interesting behaviour.

5 Conclusion

This study investigated the biogeochemical interactions between fermenting broken maize and binder materials intended for anaerobic digester structures. Four types of binder materials were inserted into reactors inoculated with broken maize during five consecutive cycles of anaerobic digestion (245 days). The presence of the cement pastes CEM I, CEM III and CAC did not influence the AD bioprocess in terms of pH, production of VFA and NH_4^+ ions, production of CH_4 nor did it influence microbial populations. CEM I and CEM III pastes nevertheless experienced biodegradation, with phenomena of decalcification, carbonation and enrichment in P_2O_5 on the surface. The CEM III paste generated a different zonation and a greater modified depth at the end of the experiment, which was probably linked to the high sensitivity of the slags when exposed to carbonation.

In contrast, alkali-activated metakaolin-based geopolymer showed better behaviour when faced with the aggressive environmental conditions, and exhibited a small modified depth, with a thickness of

several hundred micrometres only at the end of the experiment. The presence of this material led to very low NH_4^+ concentrations, probably due to these adsorption capacities, which could be beneficial for the treatment of nitrogen-rich biowaste. Moreover, the presence of the geopolymer resulted in a different microbial population (absence of the genera *Methanobacterium* and *Aminomonas)* and a slightly higher pH, although the CH_4 production was similar to that of other BMP reactors. Finally, differences were observed between sessile and planktonic populations in all BMP reactors, with more acidogens in the biofilm, mainly members of the genus *Clostridium*. The main difference observed was a greater presence of acidogens within the depth of the biofilm, especially members of the genus *Clostridium*, which were frequently encountered in the strongly adhered biofilm formed on all the materials.

CRediT authorship contribution statement

Marie Giroudon: Conceptualization; Methodology; Investigation; Validation; Writing - Original Draft; Writing - Review & Editing; Visualization

Cédric Perez: Conceptualization; Methodology; Investigation; Validation; Formal analysis; Writing - Original Draft; Writing - Review & Editing; Visualization

Matthieu Peyre Lavigne: Conceptualization; Methodology; Investigation; Resources; Writing - Review & Editing; Supervision

Benjamin Erable: Conceptualization; Methodology; Resources; Writing - Review & Editing; Supervision

Christine Lors: Conceptualization; Methodology; Writing - Review & Editing; Supervision

Cédric Patapy: Conceptualization; Methodology; Resources; Writing - Review & Editing; Supervision

Alexandra Bertron: Conceptualization; Methodology; Resources; Writing - Review & Editing; Supervision; Project administration; Funding acquisition

Declaration of competing interest

The authors declare that they know of no competing financial interests or personal relationships that could have influenced the work reported in this paper.

Acknowledgements

The authors wish to thank the French National Research Agency (ANR) for funding the project BIBENdOM – ANR – 16 – CE22 – 001 DS0602. The authors also thank Evrard Mengelle, Simon Dubos, Mansour Bounouba and Chantha Kim for the design of the pilot and the analytical support for the BMP reactors.

References

AFNOR, 2016. NF EN 196-1. Méthodes d'essais des ciments - Partie 1 : détermination des résistances. Paris, France.

AFNOR, 2010. NF P18-459. Concrete - Testing hardened concrete - Testing porosity and density. Paris, France.

Baena, S., Garcia, J.-L., Cayol, J.-L., Ollivier, B., 2015. Aminomonas, in: Bergey's Manual of Systematics of Archaea and Bacteria. American Cancer Society, pp. 1–6. https://doi.org/10.1002/9781118960608.gbm01251

Bakharev, T., 2005. Resistance of geopolymer materials to acid attack. Cem. Concr. Res. 35, 658–670. https://doi.org/10.1016/j.cemconres.2004.06.005

Baroghel-Bouny, V., Capra, B., Laurens, D., 2008. La durabilité des armatures et du béton d'enrobage, in: La Durabilité des Bétons. pp. 303–385.

Batstone, D.J., Keller, J., Angelidaki, I., Kalyuzhnyi, S.V., Pavlostathis, S.G., Rozzi, A., Sanders, W.T.M., Siegrist, H., Vavilin, V.A., 2002. The IWA Anaerobic Digestion Model No 1 (ADM1). Water Sci. Technol. 45, 65–73.

Bertron, A., Duchesne, J., 2013. Attack of Cementitious Materials by Organic Acids in Agricultural and Agrofood Effluents, in: Performance of Cement-Based Materials in Aggressive Aqueous

661 Environments, RILEM State-of-the-Art Reports. Springer, Dordrecht, pp. 131–173.
662 https://doi.org/10.1007/978-94-007-5413-3_6
663 Bertron, A., Duchesne, J., Escadeillas, G., 2007a. Durability of various binders exposed to organic
664 acids in manure. Presented at the Seventh CANMET/ACI International Conference on
665 Durability of Concrete, Montreal.
666 Bertron, A., Duchesne, J., Escadeillas, G., 2007b. Degradation of cement pastes by organic acids.
667 Mater. Struct. 40, 341–354. https://doi.org/10.1617/s11527-006-9110-3
668 Bertron, A., Duchesne, J., Escadeillas, G., 2005a. Accelerated tests of hardened cement pastes
669 alteration by organic acids: analysis of the pH effect. Cem. Concr. Res. 35, 155–166.
670 https://doi.org/10.1016/j.cemconres.2004.09.009
671 Bertron, A., Duchesne, J., Escadeillas, G., 2005b. Attack of cement pastes exposed to organic acids in
672 manure. Cem. Concr. Compos. 27, 898–909.
673 https://doi.org/10.1016/j.cemconcomp.2005.06.003
674 Bertron, A., Escadeillas, G., de Parseval, P., Duchesne, J., 2009. Processing of electron microprobe
675 data from the analysis of altered cementitious materials. Cem. Concr. Res. 39, 929–935.
676 https://doi.org/10.1016/j.cemconres.2009.06.011
677 Bertron, A., Escadeillas, G., Duchesne, J., 2004. Cement pastes alteration by liquid manure organic
678 acids: chemical and mineralogical characterization. Cem. Concr. Res. 34, 1823–1835.
679 https://doi.org/10.1016/j.cemconres.2004.01.002
680 Bertron, A., Peyre Lavigne, M., Patapy, C., Erable, B., 2017. Biodeterioration of concrete in
681 agricultural, agro-food and biogas plants: state of the art and challenges. RILEM Tech. Lett. 2,
682 83–89. https://doi.org/10.21809/rilemtechlett.2017.42
683 Board, E., 2015. Synergistaceae, in: Bergey's Manual of Systematics of Archaea and Bacteria.
684 American Cancer Society, pp. 1–1. https://doi.org/10.1002/9781118960608.fbm00243
685 Board, T.E., 2015. Petrimonas, in: Bergey's Manual of Systematics of Archaea and Bacteria. American
686 Cancer Society, pp. 1–2. https://doi.org/10.1002/9781118960608.gbm00245
687 Bond, T., Templeton, M.R., 2011. History and future of domestic biogas plants in the developing
688 world. Energy Sustain. Dev. 15, 347–354. https://doi.org/10.1016/j.esd.2011.09.003
689 Borges, P.H.R., Costa, J.O., Milestone, N.B., Lynsdale, C.J., Streatfield, R.E., 2010. Carbonation of CH
690 and C–S–H in composite cement pastes containing high amounts of BFS. Cem. Concr. Res. 40,
691 284–292. https://doi.org/10.1016/j.cemconres.2009.10.020
692 Bosshard, P.P., 2015. Turicibacter, in: Bergey's Manual of Systematics of Archaea and Bacteria.
693 American Cancer Society, pp. 1–2. https://doi.org/10.1002/9781118960608.gbm00766
694 Bruni, E., Jensen, A.P., Pedersen, E.S., Angelidaki, I., 2010. Anaerobic digestion of maize focusing on
695 variety, harvest time and pretreatment. Appl. Energy 87, 2212–2217.
696 https://doi.org/10.1016/j.apenergy.2010.01.004
697 Burciaga-Díaz, O., Escalante-García, J.I., 2012. Strength and Durability in Acid Media of Alkali Silicate-
698 Activated Metakaolin Geopolymers. J. Am. Ceram. Soc. 95, 2307–2313.
699 https://doi.org/10.1111/j.1551-2916.2012.05249.x
700 Chambre d'Agriculture, 2010. La méthanisation agricole, Fiche technique.
701 Drugă, B., Ukrainczyk, N., Weise, K., Koenders, E., Lackner, S., 2018. Interaction between wastewater
702 microorganisms and geopolymer or cementitious materials: Biofilm characterization and
703 deterioration characteristics of mortars. Int. Biodeterior. Biodegrad. 134, 58–67.
704 https://doi.org/10.1016/j.ibiod.2018.08.005
705 Duan, P., Yan, C., Zhou, W., Luo, W., Shen, C., 2015. An investigation of the microstructure and
706 durability of a fluidized bed fly ash–metakaolin geopolymer after heat and acid exposure.
707 Mater. Des. 74, 125–137. https://doi.org/10.1016/j.matdes.2015.03.009
708 Duchesne, J., Bertron, A., 2013. Leaching of Cementitious Materials by Pure Water and Strong Acids
709 (HCl and HNO3), in: Alexander, M., Bertron, A., Belie, N.D. (Eds.), Performance of Cement-
710 Based Materials in Aggressive Aqueous Environments. Springer Netherlands, pp. 91–112.

711 Escadeillas, G., 2013. Ammonium Nitrate Attack on Cementitious Materials, in: Performance of
712 Cement-Based Materials in Aggressive Aqueous Environments, RILEM State-of-the-Art
713 Reports. Springer, Dordrecht, pp. 113–130. https://doi.org/10.1007/978-94-007-5413-3_5
714 Evans, G.M., Furlong, J.C., 2003. Environmental Biotechnology - Theory and Application. John Wiley &
715 Sons.
716 Galan, I., Glasser, F.P., Baza, D., Andrade, C., 2015. Assessment of the protective effect of
717 carbonation on portlandite crystals. Cem. Concr. Res. 74, 68–77.
718 https://doi.org/10.1016/j.cemconres.2015.04.001
719 Gerin, P.A., Vliegen, F., Jossart, J.-M., 2008. Energy and CO2 balance of maize and grass as energy
720 crops for anaerobic digestion. Bioresour. Technol. 99, 2620–2627.
721 https://doi.org/10.1016/j.biortech.2007.04.049
722 Giroudon, M., Peyre Lavigne, M., Patapy, C., Bertron, A., 2021a. Blast-furnace slag cement and
723 metakaolin based geopolymer as construction materials for liquid anaerobic digestion
724 structures: Interactions and biodeterioration mechanisms. Sci. Total Environ. 750, 141518.
725 https://doi.org/10.1016/j.scitotenv.2020.141518
726 Giroudon, M., Peyre Lavigne, M., Patapy, C., Bertron, A., 2021b. Evaluation of the contribution of
727 chemical compounds to the degradation of Portland cement-based materials during
728 anaerobic digestion. J. Environ. Manage. Submitted.
729 Grengg, C., Ukrainczyk, N., Koraimann, G., Mueller, B., Dietzel, M., Mittermayr, F., 2020. Long-term in
730 situ performance of geopolymer, calcium aluminate and Portland cement-based materials
731 exposed to microbially induced acid corrosion. Cem. Concr. Res. 131, 106034.
732 https://doi.org/10.1016/j.cemconres.2020.106034
733 Gruyaert, E., Van den Heede, P., Maes, M., De Belie, N., 2012. Investigation of the influence of blast-
734 furnace slag on the resistance of concrete against organic acid or sulphate attack by means
735 of accelerated degradation tests. Cem. Concr. Res. 42, 173–185.
736 https://doi.org/10.1016/j.cemconres.2011.09.009
737 Han, J., Liang, Y., Sun, W., Liu, W., Wang, S., 2015. Microstructure Modification of Carbonated
738 Cement Paste with Six Kinds of Modern Microscopic Instruments. J. Mater. Civ. Eng. 27,
739 04014262. https://doi.org/10.1061/(ASCE)MT.1943-5533.0001210
740 Holliger, C., Alves, M., Andrade, D., Angelidaki, I., Astals, S., Baier, U., Bougrier, C., Buffière, P.,
741 Carballa, M., de Wilde, V., Ebertseder, F., Fernández, B., Ficara, E., Fotidis, I., Frigon, J.-C., de
742 Laclos, H.F., Ghasimi, D.S.M., Hack, G., Hartel, M., Heerenklage, J., Horvath, I.S., Jenicek, P.,
743 Koch, K., Krautwald, J., Lizasoain, J., Liu, J., Mosberger, L., Nistor, M., Oechsner, H., Oliveira,
744 J.V., Paterson, M., Pauss, A., Pommier, S., Porqueddu, I., Raposo, F., Ribeiro, T., Rüsch Pfund,
745 F., Strömberg, S., Torrijos, M., van Eekert, M., van Lier, J., Wedwitschka, H., Wierinck, I.,
746 2016. Towards a standardization of biomethane potential tests. Water Sci. Technol. 74,
747 2515–2522. https://doi.org/10.2166/wst.2016.336
748 Karthikeyan, O.P., Visvanathan, C., 2013. Bio-energy recovery from high-solid organic substrates by
749 dry anaerobic bio-conversion processes: a review. Rev. Environ. Sci. Biotechnol. 12, 257–284.
750 https://doi.org/10.1007/s11157-012-9304-9
751 Koenig, A., Dehn, F., 2016. Biogenic acid attack on concretes in biogas plants. Biosyst. Eng. 147, 226–
752 237. https://doi.org/10.1016/j.biosystemseng.2016.03.007
753 Krakat, N., Westphal, A., Schmidt, S., Scherer, P., 2010. Anaerobic Digestion of Renewable Biomass:
754 Thermophilic Temperature Governs Methanogen Population Dynamics. Appl. Environ.
755 Microbiol. 76, 1842–1850. https://doi.org/10.1128/AEM.02397-09
756 Langer, S., Schropp, D., Bengelsdorf, F.R., Othman, M., Kazda, M., 2014. Dynamics of biofilm
757 formation during anaerobic digestion of organic waste. Anaerobe 29, 44–51.
758 https://doi.org/10.1016/j.anaerobe.2013.11.013
759 Li, N., Farzadnia, N., Shi, C., 2017. Microstructural changes in alkali-activated slag mortars induced by
760 accelerated carbonation. Cem. Concr. Res. 100, 214–226.
761 https://doi.org/10.1016/j.cemconres.2017.07.008

762 Liu, Y., Whitman, W.B., 2008. Metabolic, Phylogenetic, and Ecological Diversity of the Methanogenic
763 Archaea. Ann. N. Y. Acad. Sci. 1125, 171–189. https://doi.org/10.1196/annals.1419.019
764 Lothenbach, B., Scrivener, K., Hooton, R.D., 2011. Supplementary cementitious materials. Cem.
765 Concr. Res., Conferences Special: Cement Hydration Kinetics and Modeling, Quebec City,
766 2009 & CONMOD10, Lausanne, 2010 41, 1244–1256.
767 https://doi.org/10.1016/j.cemconres.2010.12.001
768 Magniont, C., Coutand, M., Bertron, A., Cameleyre, X., Lafforgue, C., Beaufort, S., Escadeillas, G.,
769 2011. A new test method to assess the bacterial deterioration of cementitious materials.
770 Cem. Concr. Res. 41, 429–438. https://doi.org/10.1016/j.cemconres.2011.01.014
771 Meegoda, J., Li, B., Patel, K., Wang, L., 2018. A Review of the Processes, Parameters, and
772 Optimization of Anaerobic Digestion. Int. J. Environ. Res. Public. Health 15, 2224.
773 https://doi.org/10.3390/ijerph15102224
774 Ministère de la transition écologique et solidaire, 2020. Programmation Pluriannuelle de l'Energie
775 2019 - 2023 2024 - 2028 Stratégie française pour lénergie et le climat - Projet pour
776 consultation.
777 Nathalie Bachmann, E.S.A., 2013. 8 - Design and engineering of biogas plants, in: Wellinger, A.,
778 Murphy, J., Baxter, D. (Eds.), The Biogas Handbook, Woodhead Publishing Series in Energy.
779 Woodhead Publishing, pp. 191–211. https://doi.org/10.1533/9780857097415.2.191
780 Nedeljković, M., Šavija, B., Zuo, Y., Luković, M., Ye, G., 2018. Effect of natural carbonation on the pore
781 structure and elastic modulus of the alkali-activated fly ash and slag pastes. Constr. Build.
782 Mater. 161, 687–704. https://doi.org/10.1016/j.conbuildmat.2017.12.005
783 Ngala, V.T., Page, C.L., 1997. Effects of carbonation on pore structure and diffusional properties of
784 hydrated cement pastes. Cem. Concr. Res. 27, 995–1007. https://doi.org/10.1016/S0008-
785 8846(97)00102-6
786 Osborne, G.J., 1999. Durability of Portland blast-furnace slag cement concrete. Cem. Concr. Compos.
787 21, 11–21. https://doi.org/10.1016/S0958-9465(98)00032-8
788 Oueslati, O., Duchesne, J., 2014. Resistance of blended cement pastes subjected to organic acids:
789 Quantification of anhydrous and hydrated phases. Cem. Concr. Compos. 45, 89–101.
790 https://doi.org/10.1016/j.cemconcomp.2013.09.007
791 Oueslati, O., Duchesne, J., 2012. The effect of SCMs and curing time on resistance of mortars
792 subjected to organic acids. Cem. Concr. Res. 42, 205–214.
793 https://doi.org/10.1016/j.cemconres.2011.09.017
794 Perez, C., Lors, C., Floquet, P., Erable, B., 2021. Biodeterioration kinetics and microbial community
795 organization on surface of cementitious materials exposed to anaerobic digestion conditions.
796 J. Environ. Chem. Eng. 9, 105334. https://doi.org/10.1016/j.jece.2021.105334
797 Pouhet, R., 2015. Formulation and durability of metakaolin-based geopolymers (Thesis). Université
798 de Toulouse, Université Toulouse III - Paul Sabatier.
799 Pouhet, R., Cyr, M., Bucher, R., 2019. Influence of the initial water content in flash calcined
800 metakaolin-based geopolymer. Constr. Build. Mater. 201, 421–429.
801 https://doi.org/10.1016/j.conbuildmat.2018.12.201
802 Puertas, F., Palacios, M., Vázquez, T., 2006. Carbonation process of alkali-activated slag mortars. J.
803 Mater. Sci. 41, 3071–3082. https://doi.org/10.1007/s10853-005-1821-2
804 Sanjuán, M.Á., Estévez, E., Argiz, C., Barrio, D. del, 2018. Effect of curing time on granulated blast-
805 furnace slag cement mortars carbonation. Cem. Concr. Compos. 90, 257–265.
806 https://doi.org/10.1016/j.cemconcomp.2018.04.006
807 Šavija, B., Luković, M., 2016. Carbonation of cement paste: Understanding, challenges, and
808 opportunities. Constr. Build. Mater. 117, 285–301.
809 https://doi.org/10.1016/j.conbuildmat.2016.04.138
810 Schink, B., 2015. Pelospora, in: Bergey's Manual of Systematics of Archaea and Bacteria. American
811 Cancer Society, pp. 1–4. https://doi.org/10.1002/9781118960608.gbm00681
812 Sekiguchi, Y., 2015. *Syntrophomonas*, in: Whitman, W.B., Rainey, F., Kämpfer, P., Trujillo, M., Chun, J.,
813 DeVos, P., Hedlund, B., Dedysh, S. (Eds.), Bergey's Manual of Systematics of Archaea and

814 Bacteria. John Wiley & Sons, Ltd, Chichester, UK, pp. 1–11.
815 https://doi.org/10.1002/9781118960608.gbm00682
816 Sevelsted, T.F., Skibsted, J., 2015. Carbonation of C–S–H and C–A–S–H samples studied by 13C, 27Al
817 and 29Si MAS NMR spectroscopy. Cem. Concr. Res. 71, 56–65.
818 https://doi.org/10.1016/j.cemconres.2015.01.019
819 Shah, V., Scrivener, K., Bhattacharjee, B., Bishnoi, S., 2018. Changes in microstructure characteristics
820 of cement paste on carbonation. Cem. Concr. Res. 109, 184–197.
821 https://doi.org/10.1016/j.cemconres.2018.04.016
822 Singh, B., Ishwarya, G., Gupta, M., Bhattacharyya, S.K., 2015. Geopolymer concrete: A review of some
823 recent developments. Constr. Build. Mater. 85, 78–90.
824 https://doi.org/10.1016/j.conbuildmat.2015.03.036
825 Song, H., Clarke, W.P., Blackall, L.L., 2005. Concurrent microscopic observations and activity
826 measurements of cellulose hydrolyzing and methanogenic populations during the batch
827 anaerobic digestion of crystalline cellulose. Biotechnol. Bioeng. 91, 369–378.
828 https://doi.org/10.1002/bit.20517
829 Steiner, S., Lothenbach, B., Proske, T., Borgschulte, A., Winnefeld, F., 2020. Effect of relative humidity
830 on the carbonation rate of portlandite, calcium silicate hydrates and ettringite. Cem. Concr.
831 Res. 135, 106116. https://doi.org/10.1016/j.cemconres.2020.106116
832 Su, X.-L., Tian, Q., Zhang, J., Yuan, X.-Z., Shi, X.-S., Guo, R.-B., Qiu, Y.-L., 2014. Acetobacteroides
833 hydrogenigenes gen. nov., sp. nov., an anaerobic hydrogen-producing bacterium in the
834 family Rikenellaceae isolated from a reed swamp. Int. J. Syst. Evol. Microbiol. 64, 2986–2991.
835 https://doi.org/10.1099/ijs.0.063917-0
836 Thiery, M., Villain, G., Dangla, P., Platret, G., 2007. Investigation of the carbonation front shape on
837 cementitious materials: Effects of the chemical kinetics. Cem. Concr. Res. 37, 1047–1058.
838 https://doi.org/10.1016/j.cemconres.2007.04.002
839 Tourlousse, D.M., Sekiguchi, Y., 2018. Flexilinea, in: Bergey's Manual of Systematics of Archaea and
840 Bacteria. American Cancer Society, pp. 1–4.
841 https://doi.org/10.1002/9781118960608.gbm01551
842 Ukrainczyk, N., Vogt, O., 2020. Geopolymer leaching in water and acetic acid. RILEM Tech. Lett. 5,
843 163–173. https://doi.org/10.21809/rilemtechlett.2020.124
844 Venkiteshwaran, K., Bocher, B., Maki, J., Zitomer, D., 2015. Relating Anaerobic Digestion Microbial
845 Community and Process Function : Supplementary Issue: Water Microbiology. Microbiol.
846 Insights 8s2, MBI.S33593. https://doi.org/10.4137/MBI.S33593
847 Voegel, C., Bertron, A., Erable, B., 2016. Mechanisms of cementitious material deterioration in biogas
848 digester. Sci. Total Environ. 571, 892–901. https://doi.org/10.1016/j.scitotenv.2016.07.072
849 Voegel, C., Durban, N., Bertron, A., Landon, Y., Erable, B., 2020. Evaluation of microbial proliferation
850 on cementitious materials exposed to biogas systems. Environ. Technol. 41, 2439–2449.
851 https://doi.org/10.1080/09593330.2019.1567610
852 Voegel, C., Giroudon, M., Bertron, A., Patapy, C., Peyre Lavigne, M., Verdier, T., Erable, B., 2019.
853 Cementitious materials in biogas systems: Biodeterioration mechanisms and kinetics in CEM I
854 and CAC based materials. Cem. Concr. Res. 124, 105815.
855 https://doi.org/10.1016/j.cemconres.2019.105815
856 Yoon, S.S., Hennigan, R.F., Hilliard, G.M., Ochsner, U.A., Parvatiyar, K., Kamani, M.C., Allen, H.L.,
857 DeKievit, T.R., Gardner, P.R., Schwab, U., Rowe, J.J., Iglewski, B.H., McDermott, T.R., Mason,
858 R.P., Wozniak, D.J., Hancock, R.E.W., Parsek, M.R., Noah, T.L., Boucher, R.C., Hassett, D.J.,
859 2002. Pseudomonas aeruginosa Anaerobic Respiration in Biofilms: Relationships to Cystic
860 Fibrosis Pathogenesis. Dev. Cell 3(4), 593–603.
861

862

Supplementary material

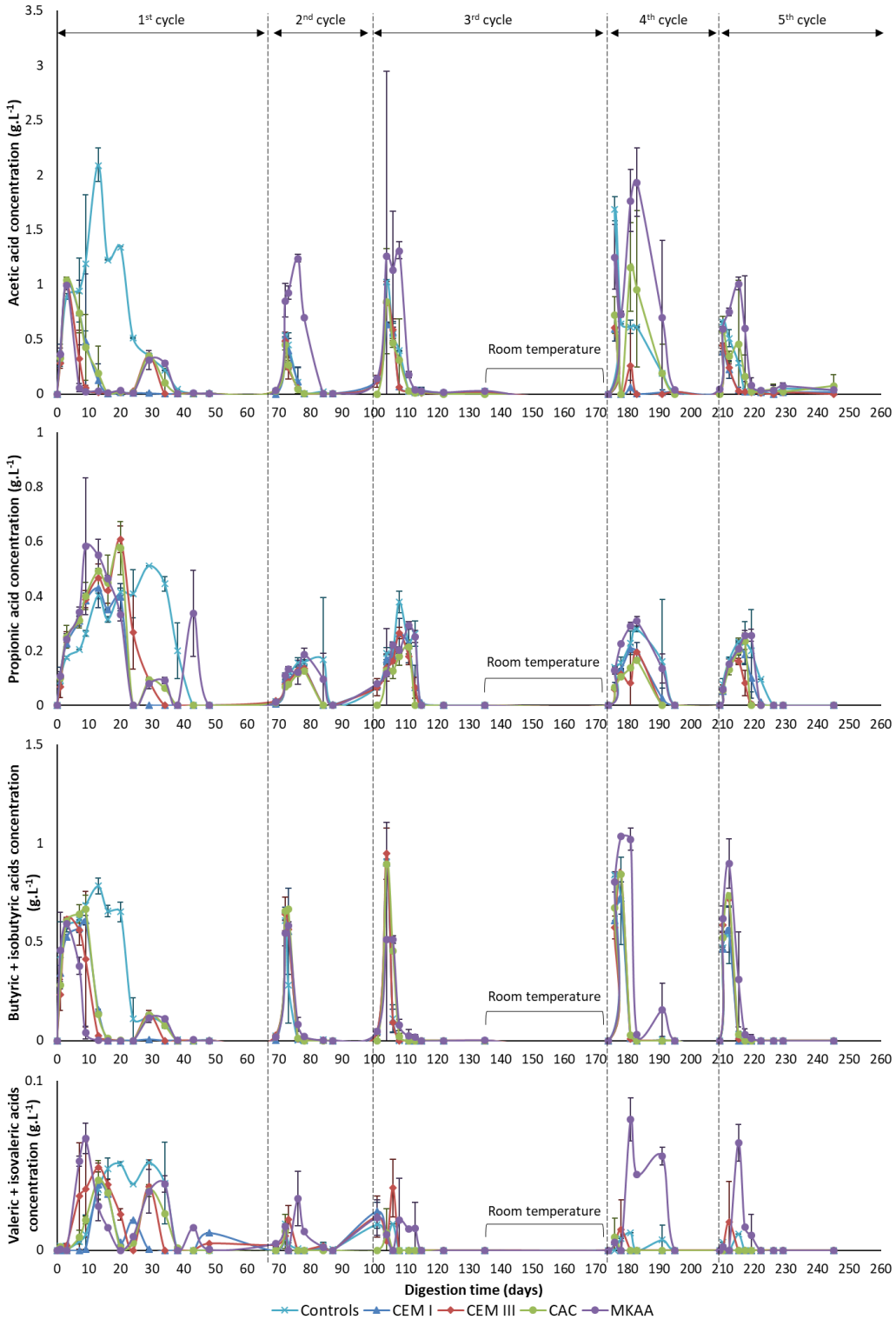

Appendix A: Evolution of the VFA concentrations during the five cycles of AD in the BMP reactors, with or without binder materials. Mean values of the two duplicate BMP reactors are presented with the standard deviations.

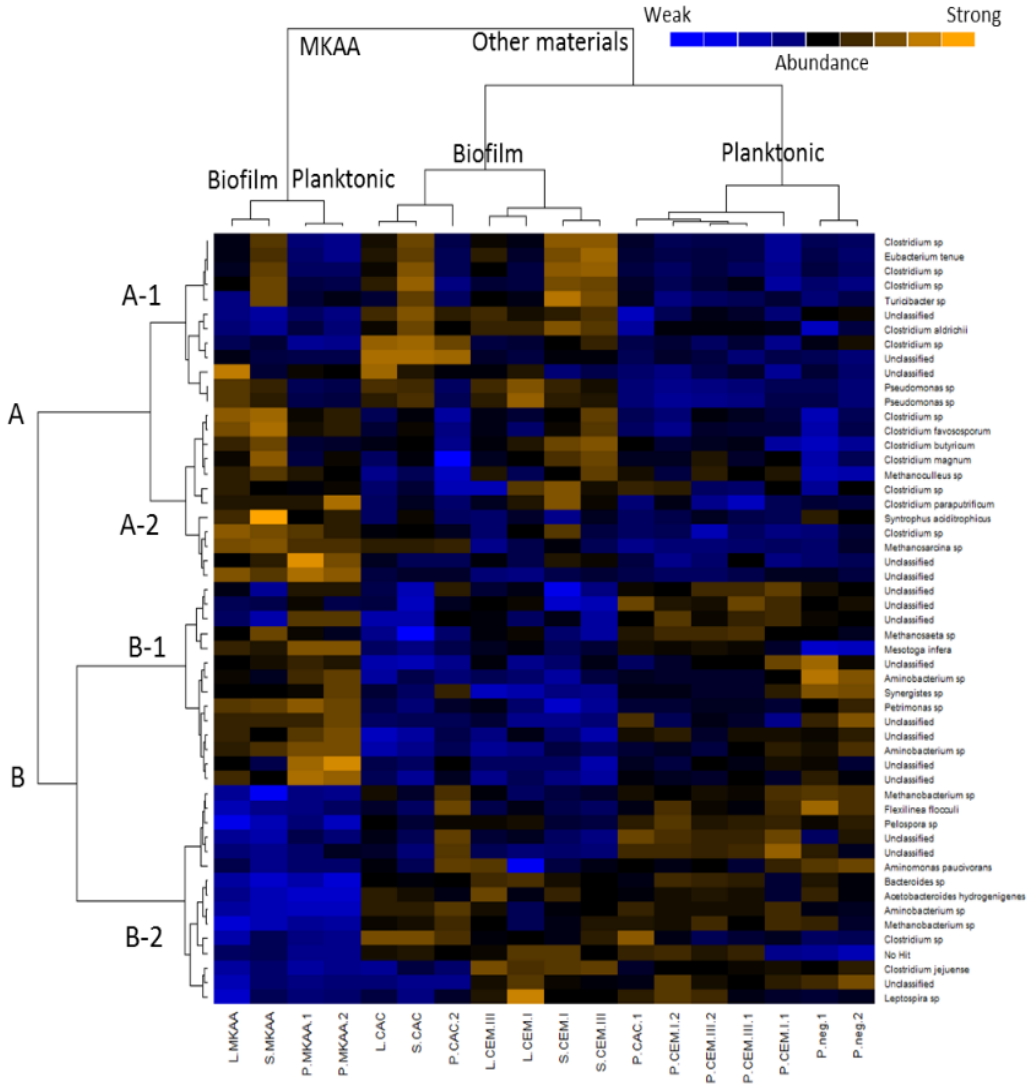

Appendix B: Heatmap with colour scale of the next generation sequencing of the 16S DNA from planktonic biomass samples and "poorly" and "strongly" adhered biomass taken from the surface of cementitious material samples and after 5 cycles of anaerobic digestion – L: weakly adhered biofilm; S: Strongly adhered biofilm; P: Planktonic; only OTUs with an abundance of at least 1% in at least one sample are shown

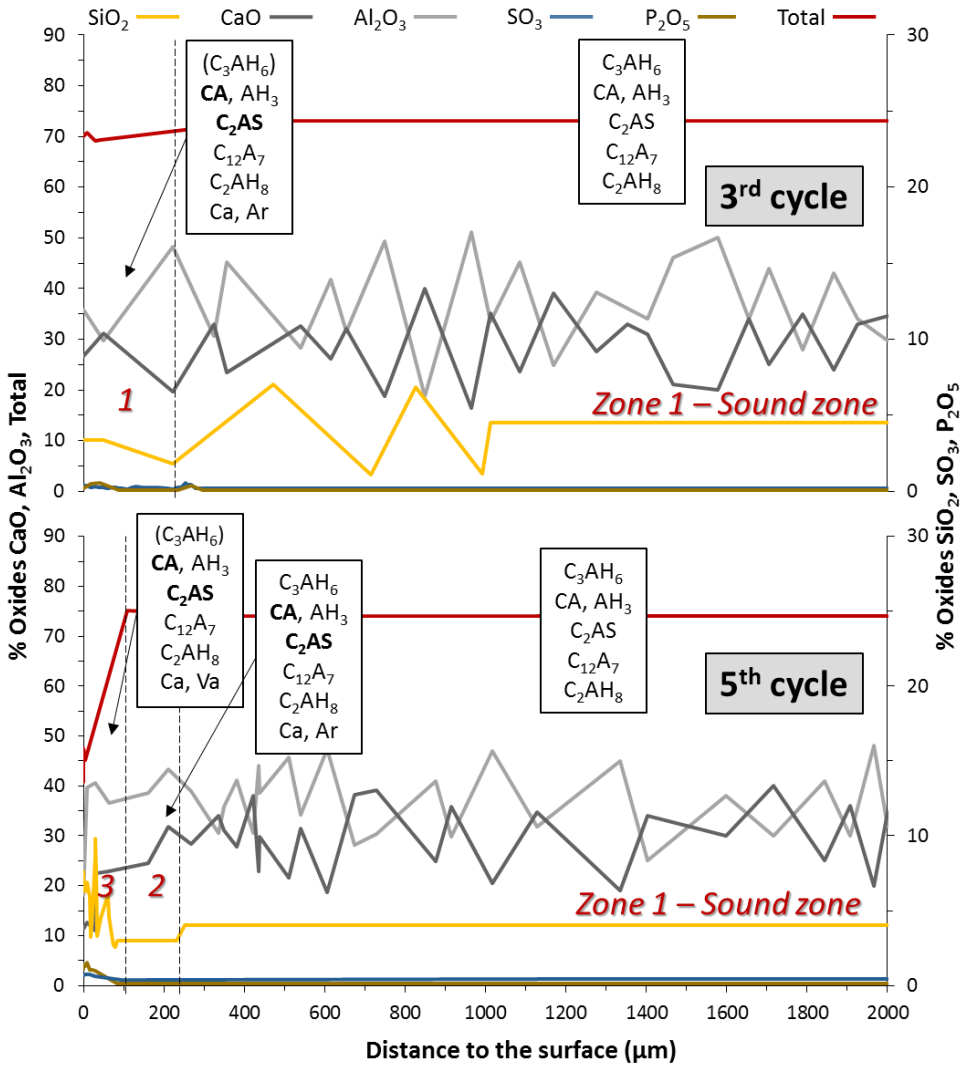

873

874 *Appendix C: Chemical (EPMA) and mineralogical (XRD) changes in the CAC pastes after 3 and 5 cycles of anaerobic digestion*
875 *of broken maize – Ca: calcite; Ar: aragonite – Bold characters = intensification of the XRD signal in comparison with the*
876 *deeper zone; Parentheses = significantly lower intensity of the XRD signal in comparison with the main phase*

877

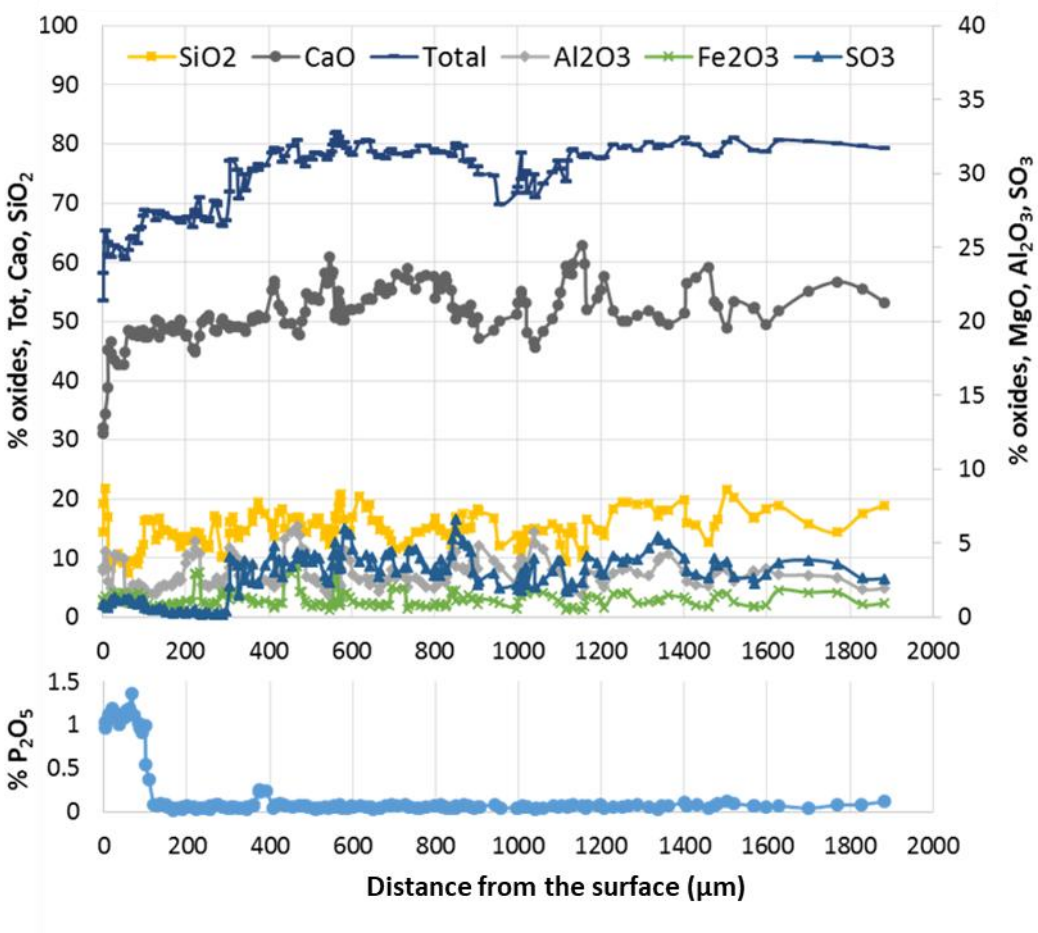

878

879 *Appendix D: Chemical composition profile (EPMA), according to the distance from the surface, of the CEM I paste after 5*
880 *cycles in the broken maize in digestion*

881

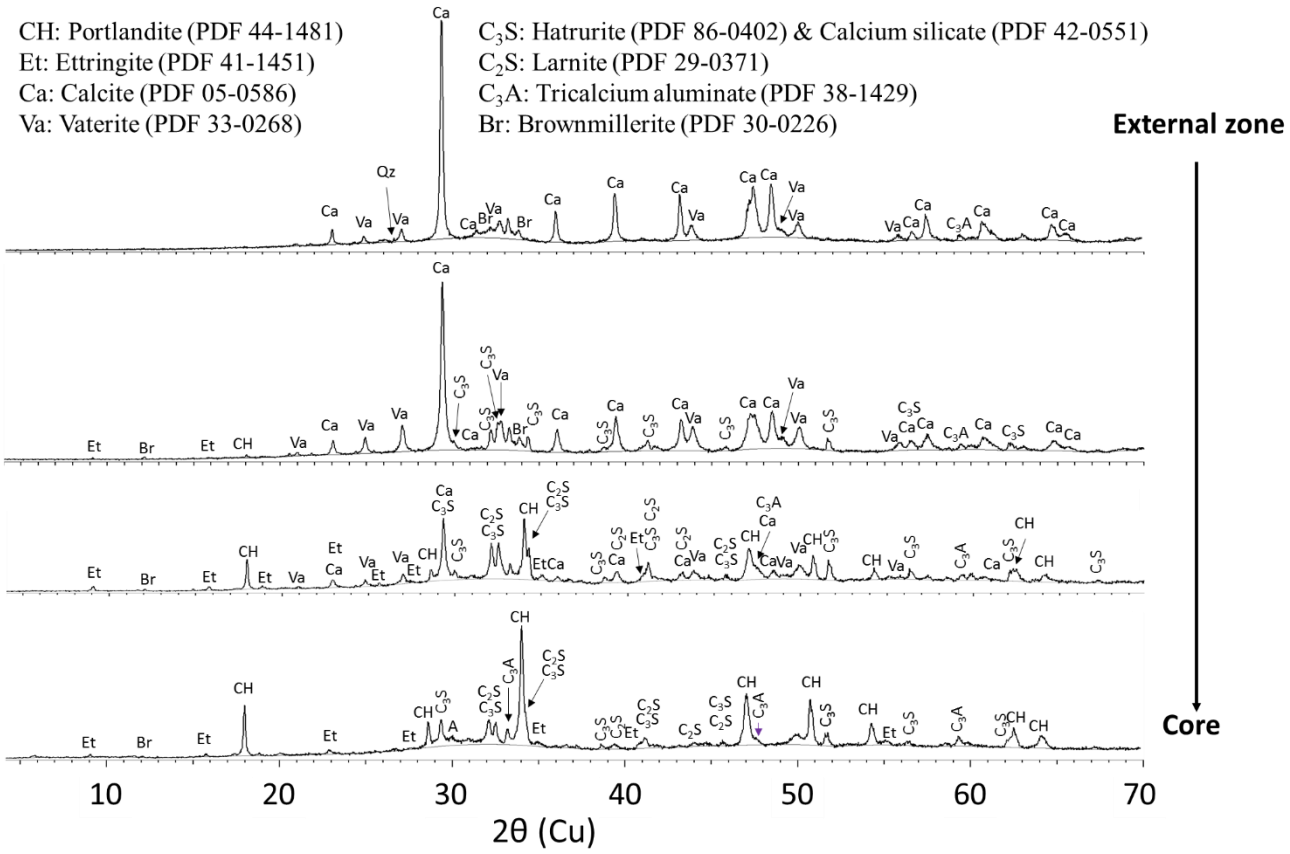

882

883 *Appendix E: Mineralogical analyses of the CEM I paste after 5 cycles in the fermenting broken maize*

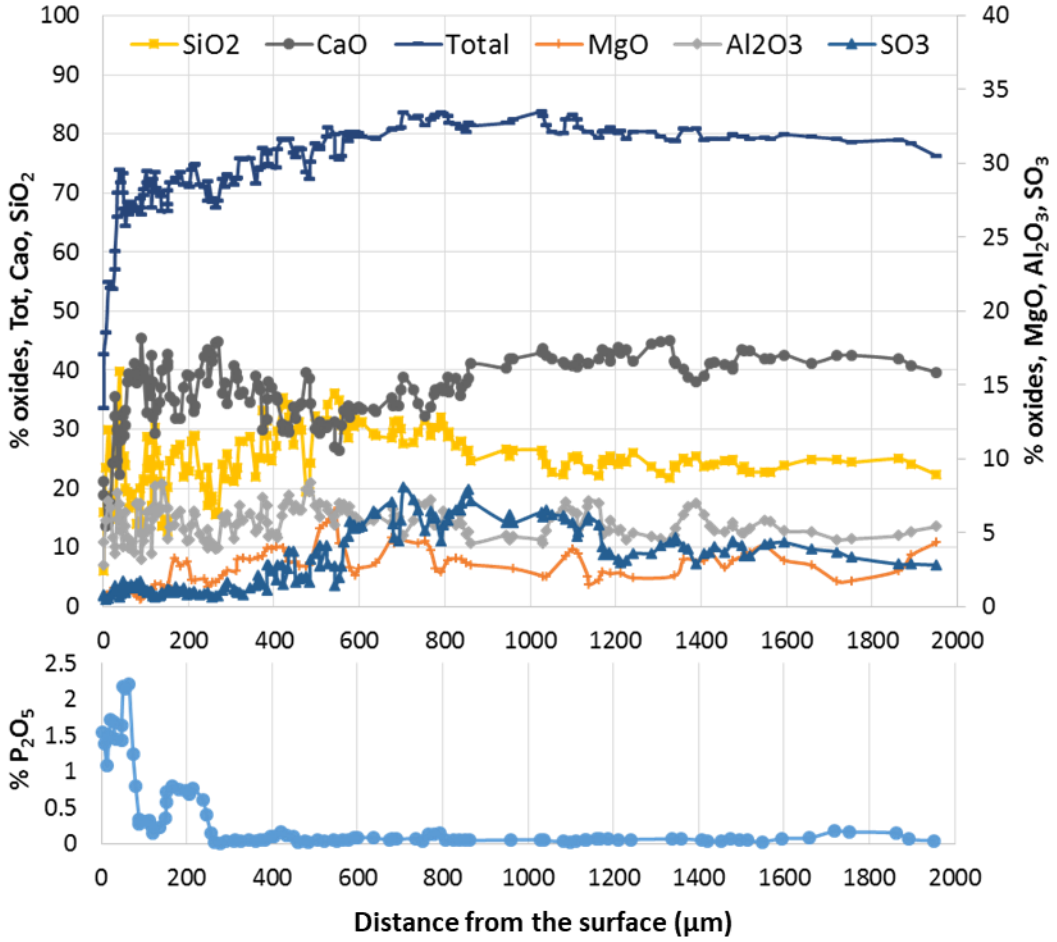

884

885 *Appendix F: Chemical composition profile (EPMA), according to the distance from the surface, of the CEM III paste after 5*
886 *cycles in the fermenting broken maize*

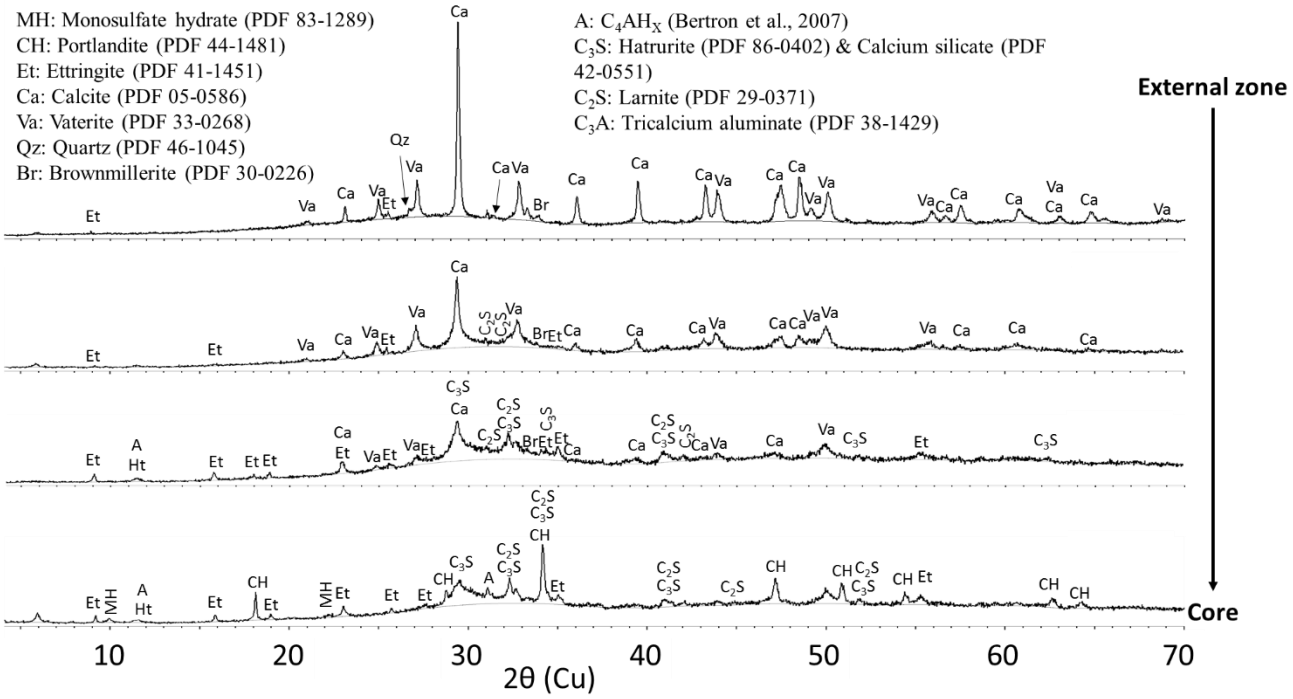

887

888 *Appendix G: Mineralogical analyses of the CEM III paste after 5 cycles in the fermenting broken maize, C_4AH_X identification*
889 *from Bertron et al. (2007b)*

890

891 **RT-LABS Amplification and Sequencing protocol**

892 **Illumina 2-step**

893 Samples were amplified for sequencing in a two-step process. The forward primer was constructed
894 (5'-3') with the forward Illumina overhang adapter (TCGTCGGCAGCGTCAGATGTGTATAAGAGACAG)
895 added to the 515F primer (GTGCCAGCMGCCGCGGTAA). The reverse primer was constructed (5'-3')
896 with the reverse Illumina overhang adapter (GTCTCGTGGGCTCGGAGATGTGTATAAGAGACAG) added
897 to the 806R primer (GGACTACHVGGGTWTCTAAT). Amplifications were performed in 25 µL reactions
898 with Qiagen HotStar Taq master mix (Qiagen Inc., Valencia, California), 1 µL of each 5 µM primer and
899 1 µL of template. Reactions were performed on ABI Veriti thermocyclers (Applied Biosytems,
900 Carlsbad, California) under the following thermal profile: 95 °C for 5 min, then 35 cycles of 94 °C for
901 30 s, 54 °C for 40 s, 72 °C for 1 min, followed by one cycle of 72 °C for 10 min and 4 °C hold.

Products from the first stage amplification were added to a second PCR based on qualitatively determined concentrations. Primers for the second PCR were designed based on the Illumina Nextera PCR primers as follows: Forward - AATGATACGGCGACCACCGAGATCTACAC[i5index]TCGTCGGCAGCGTC and Reverse - CAAGCAGAAGACGGCATACGAGAT[i7index]GTCTCGTGGGCTCGG. The second stage amplification was run in the same way as the first stage except for 10 cycles.

Amplification products were visualized with eGels (Life Technologies, Grand Island, New York). Products were then pooled at equimolar ratios and each pool was size selected in two rounds using SPRIselect Reagent (BeckmanCoulter, Indianapolis, Indiana) in a 0.75 ratio for both rounds. Size selected pools were then quantified using the Qubit 4 Fluorometer (Life Technologies) and loaded on an Illumina MiSeq (Illumina, Inc. San Diego, California) 2x300 flow cell at 10 pM.